



HAL
open science

Lysine 27 of histone H3.3 is a fine modulator of developmental gene expression and stands as an epigenetic checkpoint for lignin biosynthesis in Arabidopsis

Kateryna Fal, Alexandre Berr, Marie Le Masson, Adi Faigenboim, Emeline Pano, Nickolay Ishkhneli, Netta-lee Moyal, Claire Villette, Denisa Tomkova, Marie-edith Chabouté, et al.

► **To cite this version:**

Kateryna Fal, Alexandre Berr, Marie Le Masson, Adi Faigenboim, Emeline Pano, et al.. Lysine 27 of histone H3.3 is a fine modulator of developmental gene expression and stands as an epigenetic checkpoint for lignin biosynthesis in Arabidopsis. *New Phytologist*, 2023, 238, pp.1085-1100. 10.1111/nph.18666 . hal-04031763v2

HAL Id: hal-04031763







<https://hal.science/hal-04031763v2>

Submitted on 16 Mar 2023

HAL is a multi-disciplinary open access archive for the deposit and dissemination of scientific research documents, whether they are published or not. The documents may come from teaching and research institutions in France or abroad, or from public or private research centers.

L'archive ouverte pluridisciplinaire **HAL**, est destinée au dépôt et à la diffusion de documents scientifiques de niveau recherche, publiés ou non, émanant des établissements d'enseignement et de recherche français ou étrangers, des laboratoires publics ou privés.

Lysine 27 of histone H3.3 is a fine modulator of developmental gene expression and stands as an epigenetic checkpoint for lignin biosynthesis in *Arabidopsis*

Kateryna Fal¹ , Alexandre Berr² , Marie Le Masson¹, Adi Faigenboim³, Emeline Pano¹, Nickolay Ishkneli⁴, Netta-Lee Moyal⁴, Claire Villette² , Denisa Tomkova², Marie-Edith Chabouté² , Leor Eshed Williams⁴  and Cristel C. Carles¹ 

¹Plant and Cell Physiology Lab, IRIG-DBSCL-LPCV, CEA, Grenoble Alpes University – CNRS – INRAE – CEA, 17 rue des Martyrs, bât. C2, 38054 Grenoble Cedex 9, France; ²Institut de Biologie Moléculaire des Plantes du CNRS, Université de Strasbourg, 12 rue du Général Zimmer, 67084 Strasbourg Cedex, France; ³Institute of Plant Sciences, ARO Volcani Center, PO Box 15159, Rishon LeZion 7528809, Israel; ⁴Robert H. Smith Institute of Plant Sciences & Genetics in Agriculture – Hebrew University of Jerusalem, Rehovot 76100, Israel

Summary

Author for correspondence:

Cristel C. Carles

Email: christel.carles@univ-grenoble-alpes.fr

Received: 20 October 2022

Accepted: 28 November 2022

New Phytologist (2023)

doi: 10.1111/nph.18666

Key words: development, flowering, gene expression, histone 3, lysine residue, methylation, tissue regeneration, xylem.

• Chromatin is a dynamic platform within which gene expression is controlled by epigenetic modifications, notably targeting amino acid residues of histone H3. Among them is lysine 27 of H3 (H3K27), the trimethylation of which by the Polycomb Repressive Complex 2 (PRC2) is instrumental in regulating spatiotemporal patterns of key developmental genes. H3K27 is also subjected to acetylation and is found at sites of active transcription. Most information on the function of histone residues and their associated modifications in plants was obtained from studies of loss-of-function mutants for the complexes that modify them.

• To decrypt the genuine function of H3K27, we expressed a non-modifiable variant of H3 at residue K27 (H3.3^{K27A}) in *Arabidopsis*, and developed a multi-scale approach combining in-depth phenotypical and cytological analyses, with transcriptomics and metabolomics.

• We uncovered that the H3.3^{K27A} variant causes severe developmental defects, part of them are reminiscent of PRC2 mutants, part of them are new. They include early flowering, increased callus formation and short stems with thicker xylem cell layer. This latest phenotype correlates with mis-regulation of phenylpropanoid biosynthesis.

• Overall, our results reveal novel roles of H3K27 in plant cell fates and metabolic pathways, and highlight an epigenetic control point for elongation and lignin composition of the stem.

Introduction

Histone proteins, core components of chromatin in Eukaryotes, play key roles in the development of multi-cellular organisms by regulating DNA accessibility to the transcriptional machinery. These roles particularly take anchor on lysine residues of histones that can be dynamically modified by writers, which catalyse different types of post-translational modifications including acetylation and methylation. These modifications can either impact directly DNA–histone interactions (e.g. acetylation) or can be recognized as marks (e.g. methylation) by specific readers, for further regulation of gene accessibility and transcriptional control.

Two key antagonistic complexes, the Polycomb group (PcG) and trithorax group (trxG), catalyse the deposition of methyl groups on histone 3 lysine amino acids. Lysines 4 and 36 (H3K4/K36) can be trimethylated by trxG, forming an active mark for gene transcription, while H3K27 can be trimethylated by the PcG Repressive Complex 2 (PRC2), providing a repressive mark for gene transcription.

Historically, the PcG functions were discovered from mutants in *Drosophila* that displayed homeotic conversions due to ectopic de-repression of *Hox* genes, while the trxG functions were initially identified from mutants that rescue such PcG phenotypes (Ingham, 1983; Klymenko & Muller, 2004). Beyond this genetic antagonism, molecular characterization of trxG and PcG functions brought further evidence for their opposed actions on gene transcription (Grimaud *et al.*, 2006; Schuettengruber *et al.*, 2007). Moreover, the marks brought at targets by PRC2 and trxG histone methyl transferases (HMTs) are mutually exclusive, through direct prevention of each other's enzymatic activity (Schmitges *et al.*, 2011; Finogenova *et al.*, 2020). PRC2 and trxG activities have counterparts in plants, the PRC2 complex being the best conserved (Engelhorn *et al.*, 2014; Bieluszewski *et al.*, 2021; Baile *et al.*, 2022); however, differently from animals, most PRC2 mutants are viable in plants, likely due to redundancies of factors and multiplicity of complexes (Mozgova & Hennig, 2015; Shu *et al.*, 2020; Bieluszewski *et al.*, 2021; Godwin & Farrona, 2022).

In *Arabidopsis*, the two sporophytic homologues of the *Drosophila* E(z) HMT, CURLY LEAF (CLF) and SWINGER (SWN), are responsible for the trimethylation of H3K27 at thousands of target genes, thereby preventing their ectopic transcription (Shu *et al.*, 2019). CLF and SWN are partially redundant, having a subset of common target genes predominantly involved in plant growth and development functions, as well as in stimuli responses (Derkacheva & Hennig, 2014; Shu *et al.*, 2019). PRC2 targets are also over-represented with transcription factors (TFs). Yet, while *clf* mutants exhibit dwarf stature, curled leaves and early flowering phenotype (Goodrich *et al.*, 1997), *swn* mutants display moderate late-flowering phenotypes with no other visible defects (Shu *et al.*, 2019, 2020). Loss of both CLF and SWN, though, leads to total loss of body plan and formation of massive somatic embryo-like structures, due to the incapacity of cells to adopt proper fates (Mozgova *et al.*, 2017). Loss of function of EMF2, another *Arabidopsis* PRC2 sub-unit, homologue of the *Drosophila* Su(z)12 protein and containing a VEFS (VRN2-EMF2-FIS2-Su(z)12) domain, leads to direct flowering upon germination and sterility (Chanvivattana *et al.*, 2004). Thus, despite our knowledge of PRC2 components in plants, the plurality of sub-units, may they be redundant or alternative, does not allow to get a clear idea of the function of the deposited marks themselves (Fal *et al.*, 2021).

Compared to HMTs, our knowledge of enzymes responsible for acetylation at H3K27 is sparse, with studies in *Arabidopsis* reporting GCN5 and TAF1/HAF2 as two histone acetyl transferases, required for H3K9, H3K27 and/or H4K12 acetylation at promoters of *Arabidopsis*. While GCN5 and TAF1/HAF2 have cumulative effects mainly on H3K9 acetylation, H3K14 acetylation seems to depend only on GCN5 (Benhamed *et al.*, 2006). Mutations in *GCN5* and/or *TAF1* cause a long-hypocotyl phenotype and reduced light-inducible gene expression. GCN5 is also involved in cold response, shoot apex identity, leaf cell differentiation, root growth and flower morphogenesis (Bertrand *et al.*, 2003, 2005; Servet *et al.*, 2010; Poullos & Vlachonassios, 2018). However, direct target genes of GCN5 and TAF1/HAF2, responsible for these functions, are poorly documented except light-regulated genes (Bertrand *et al.*, 2003; Servet *et al.*, 2010).

In summary, most information on the function of histone residues and their associated marks in plants was obtained from studies of loss-of-function mutants in the complexes that modify them. However, such approaches present limits because these complexes are involved into multifaceted interactions, they display redundancies and are not always specific to a single histone residue. Moreover, total loss of some enzymatic activities (e.g. *clf* *swn*) causes dramatic phenotypes, preventing to reach a comprehensive functional information.

Several studies in animals (*Drosophila* and mammals) have explored the effect of mutations at lysine residues in histone 3, providing powerful tools to interrogate their roles *in vivo*. Such analyses were extensively done for H3K4, K36 and K27 (Trovato *et al.*, 2020). In particular, the lysine-to-methionine substitution at K27 shows a dominant phenotype due to its prevailing inhibitory effect on PRC2 HMT (Chan *et al.*, 2013; Herz *et al.*, 2014; Fang *et al.*, 2018), thereby contributing to better understand

the structural basis of H3K27me3 spreading (Justin *et al.*, 2016). Some other studies have used more neutral substitutions with amino acids such as alanine, revealing interesting effects on gene regulation and development (Pengelly *et al.*, 2013; Leatham-Jensen *et al.*, 2019; W. Zhang *et al.*, 2019; Gehre *et al.*, 2020; Trovato *et al.*, 2020). By contrast, a limited amount of studies reported similar approaches in plants (Iwakawa *et al.*, 2017; Sanders *et al.*, 2017; Lin *et al.*, 2018; Lu *et al.*, 2018; Yan *et al.*, 2020) and none of them characterized the effect of a single amino acid substitution at K27 of the ubiquitous H3 proteins, on plant growth and development. Therefore, to reveal its true function, we produced *Arabidopsis thaliana* plants that express a variant of histone 3 lacking this residue (the H3.3^{K27A} variant). We analysed the obtained lines with an integrated strategy, including quantitative phenotyping, histological and cytological analyses, as well as transcriptomics and metabolomics.

We found that developmental and molecular phenotypes of the H3.3^{K27A} *Arabidopsis* lines recapitulate some of the characteristics reported for loss-of-function in H3K27 modifiers, notably PRC2 mutants. This is particularly true for flowering time and leaf morphology, and the correlated expression of responsible TFs. Nonetheless, our dataset also highlighted features unreported thus far, such as strong defects in cell type distribution at the stem, and in related enzymatic pathway components essential for lignin biosynthesis.

Materials and Methods

Plant material and growth conditions

The *Arabidopsis thaliana* plants (*Landsberg erecta* ecotype, Ler) were grown in growth chambers at 21°C under long-day (LD; 16 h : 8 h, light : dark), and for flowering time analyses, as well under medium-day (MD; 12 h : 12 h, light : dark), short-day (SD; 8 h : 16 h, light : dark) or continuous light (CL; 24 h, light).

Construction and selection of transgenic lines

The H3.3 and H3.3^{K27A}-encoding DNA fragments were designed from the *HTR5* (At4g40040) gene and obtained by gene synthesis. They include introns, known to be essential to drive the expression of H3.3-encoding genes throughout the cell cycle (Chaubet-Gigot *et al.*, 2001). The fragments were inserted into pENTR-D-Topo, transferred into pK2WG7 and transformed into *Arabidopsis* plants by floral dip (Clough & Bent, 1998). Procedures for plant transformation, primary transformant selection and transgene expression analyses are provided as Supporting Information Methods S1.

Morphological analyses

Organogenetic measurements The lengths of inflorescence stems, quantity of side branches and number of siliques were quantified on plants with fully elongated main stems after all flowers were opened.

Shoot apical meristem sizes were measured on freshly dissected meristems, sampled after the opening of the first flower (Smyth *et al.*, 1990). Samples were imaged using a Keyence Digital Microscope VHX-5000 and analysed with Fiji (Schindelin *et al.*, 2012), as previously described (Besnard *et al.*, 2014).

Histological staining for inflorescence stems Sections (0.5–0.8 cm) from the first internode of inflorescence stems from 30-d-old plants were collected, fixed and embedded in paraplast as previously described (Carles *et al.*, 2010). The toluidine blue and phloroglucinol stainings were performed as previously described (Pradhan Mitra & Loqué, 2014).

Images were acquired using a Zeiss Imager M2 microscope equipped with an Axiocam 503. All measurements were performed with Fiji. Images of tissue sections stained with phloroglucinol were used for xylem cell size assessment, with the 3D Objects Counter plugin.

Statistical analyses Plots of all presented datasets were prepared using the RSTUDIO TEAM software (<http://www.rstudio.com/>). Tukey's range test was used to make the pairwise comparisons of means from independent samples.

Scanning electron microscopy Scanning electron microscopy (SEM) analysis was performed as previously described (Talbot & White, 2013) using a JSM-IT100 SEM (Jeol Ltd, Tokyo, Japan). In short, fresh tissue was fixed in 100% methanol for 10 min, rinsed in 100% ethanol, dried in a K850 critical point dryer and mounted on stubs and coated with a thin layer (2 nm) of gold-palladium in a Q150T ES (Quorum Technologies Ltd, Lewes, UK) for SEM imaging.

Flowering time analyses

Analyses were performed as previously described (Berr *et al.*, 2015), using two different indicators, the number of days to flowering as a temporal indicator and the leaf number at bolting as a morphometric/developmental indicator.

Callus formation and regeneration assays

To generate callus, surface-sterilized seeds were sown on MS medium (2% sucrose, 0.8% agar [pH 5.8]; Murashige & Skoog, 1962) and cultured under CL at 23°C. After 16 d, leaves number 3 and 4 were trimmed and transferred to callus-inducing medium (CIM: Gamborg B5 medium 3.2 g l⁻¹, with 0.5 g l⁻¹ MES, 2% dextrose, 0.9% phytagel, 2.2 μM 2,4-dichlorophenoxyacetic acid (2,4-D) and 0.46 μM kinetin). Plates were placed in the dark, at 23°C for 7 d, and leaves were further dissected and transferred to a new CIM plate. Calli were re-cultured once a week. All analyses were done on 30-d-old calli.

To test the capacity of 30-d old leaf-derived calli to regenerate shoots, they were transferred to shoot-inducing media (SIM: 4.4 μM 6-(γ,γ-dimethylallylamino)purine (2iP) and 0.5 μM 1-naphthylacetic acid), placed under continuous light at 23°C and imaged using a Leica M205 stereomicroscope.

Protein extraction and immunoblotting

Fractions of soluble/insoluble proteins (Schalk *et al.*, 2017) and nuclear protein extracts for histone modification analyses (Zhang *et al.*, 2020) were prepared as described previously (see Methods S1 for details). Proteins were separated by 15% SDS-PAGE, transferred onto Immobilon-P membranes (Millipore) using a Trans-Blot cell (Bio-Rad) and analysed by immunoblotting. Antibodies used in this study were anti-UGPase (AS05 086; Agrisera, Vännäs, Sweden), anti-H3 (C15200011; Diagenode, Liège, Belgique), anti-trimethyl-H3K27 (C15200181; Diagenode), anti-trimethyl-H3K4 (07–473; Millipore), anti-monomethyl-H3K27 (C15410045; Diagenode) or anti-acetyl-H3K27 (C15200184; Diagenode).

RT-qPCR

RNA was extracted using the Qiagen plant RNeasy Plant Mini Kit (ID: 74904) and reverse-transcribed to cDNA using Super-Script IV VILO (11756050; ThermoFisher Scientific, Waltham, MA USA). The relative transcript abundance was determined using the CYBR Green Master Mix (Power SYBR Green PCR, 10658255; ThermoFisher Scientific) on a CFX Connect BioRad Real-Time PCR System. Gene-specific primers used for amplification are listed in Table S1.

RNA-seq for transcriptomic analyses

RNA was extracted from 30-d-old calli, using Qiagen plant RNeasy Plant Mini Kit (ID: 74904) and treated with Turbo DNase kit (Invitrogen). RNA sequencing was performed by Macrogen Inc. (Seoul, Republic of Korea) as follows: RNA quality analysis using the 2200 TapeStation System (Agilent Technologies, Santa Clara, CA, USA), mRNA enrichment, library preparation using Illumina TruSeq RNA Library v.2 kit and 50 bp single-end sequencing on Illumina NovaSeq. The pipeline for treatment and analysis of raw-reads is provided as Methods S1.

Genes with an adjusted *P*-value ≤ 0.05 were considered differentially expressed. Pie charts for gene ontology (GO) were drawn from data outputs obtained with the Panther Classification system (<http://pantherdb.org>). For genes belonging to the 'Metabolite Interconversion Enzyme' GO, the KOBAS 3.0 tool (<http://kobas.cbi.pku.edu.cn/kobas3/?t=1>) and the KEGG PATHWAY module (Kanehisa, 2004) were used to detect statistical enrichments in pathways mapped to the KEGG database (<https://www.genome.jp/kegg/>).

Mass spectrometry for non-targeted metabolomic analyses

Metabolite extraction and analysis was performed on leaf material from 10-d-old seedlings as previously described (Villette *et al.*, 2018) using liquid chromatography coupled to high-resolution mass spectrometry on an UltiMate 3000 system (ThermoFisher Scientific) coupled to an Impact II (Bruker, Billerica, MA, USA) quadrupole time-of-flight spectrometer. Annotations for analyte lists were derived from PHENOL EXPLORER (<http://phenol-explorer.eu/>), LIPIDMAPS (<https://www.lipidmaps.org/>),

PLANTCYC (<https://plantcyc.org/>) and KNAPSACK (<http://www.knapsackfamily.com/>). Principal component analysis (PCA) was performed using METABOANALYST 5.0. Other statistical analyses were performed in METABOSCAPE 4.0 with eight different samples per genotype using the areas of the peaks as the unit of reference. A Wilcoxon rank-sum test was used to compare the different plant extracts and allow the enrichment analysis with a *P*-value set at 0.05 and a minimum fold change at (\pm) 2. The KEGG PATHWAY module (Kanehisa, 2004) was used to identify the enrichment in metabolic pathways.

Results

Arabidopsis plants expressing the H3K27A mutant display short stature, early flowering and improved callus production capacity

To address the importance of the histone 3 lysine 27 residue in plant development and gene expression, we expressed an artificial H3.3 variant in *A. thaliana*, substituting the lysine residue with an alanine (H3.3^{K27A}; Figs 1a,b, S1). We postulated that this strategy should allow to discover novel, genuine functions for the H3K27 residue and its associated marks.

A total of 21 control lines expressing the non-mutated H3.3 (hereafter named H3.3) were undistinguishable from their non-transformed Ler wild-type (WT) background. On the other hand, 14/31 plants expressing the H3.3^{K27A} variant displayed striking developmental phenotypes, including reduction in stem length and leaf defects, both consistent for all lines (Fig. S2a,b). The stem elongation defects among the 14 H3.3^{K27A} lines could be organized into three classes: no stem elongation (4 lines with stems < 1 cm at mature stage; e.g. line #D), short stems (8 lines with stems < 7 cm at mature stage; e.g. line #B) and medium-size stems (2 lines with stems < 15 cm at mature stage; e.g. line #37). Introduction of translationally silent polymorphic sequences in the H3.3-encoding transgenes allowed to identify lines with equivalent level of transgene expression, for comparative analyses between control H3.3 and artificial H3.3^{K27A} variants (Figs S1, S2c; Table S2). For all lines, the short stem phenotype intensity correlates positively with the leaf morphology defects – twisted leaves – (Figs 1c, S2a,b), as well as with the expression level of the H3.3^{K27A} transgene (Fig. S2c).

As a result of the transgene expression, a substantial amount of unmethylated H3 proteins was detectable in the soluble fraction, for the H3.3 control and H3.3^{K27A} transgenic lines (Fig. S2d). Moreover, as previously described for the developmental phenotypes, quantities of soluble H3 proteins correlate positively with the expression level of the transgene (Fig. S2c,d). Because phenotypes of the control H3.3 lines were indistinguishable from those of WT plants, the increased amount of soluble H3 proteins may not be responsible for the severely impaired phenotypes of the H3.3^{K27A} lines. Remarkably, the H3.3^{K27A} transgenic lines, but not the H3.3 control lines, displayed a lower amount of H3K27me3 in the insoluble fraction, expected to correspond to the nucleosome-loaded H3 proteins (Figs 1b, S2d).

Expression of the H3.3^{K27A} variant also impacted the floral transition, inducing early flowering, as indicated by numbers of

leaves and number of days at bolting (Figs 1d, S3). While the control H3.3 line flowered similarly to the WT plants, the H3.3^{K27A} variant provoked an early-flowering phenotype, yet less severe than the PRC2 mutant *clf-2* (Fig. S3; Carles & Fletcher, 2009). Here again, the severity of the flowering phenotype correlates with the expression level of the mutated H3.3 transgene (Fig. S3). Early flowering could be observed in SD, MD and LD conditions for the H3.3^{K27A} lines, but not under CL (Figs 1d, S3). This indicates that both tested H3.3^{K27A} lines retained a photoperiodic response. Supporting the flowering phenotypes, the transcript levels of the flowering repressors *MAF1*, *MAF2* and *FLC* (Ratcliffe *et al.*, 2003) were similarly reduced in both H3.3^{K27A} lines and in *clf-2*, as compared to the control H3.3 line and WT plants (Fig. S4). However, while the transcript levels of both *FT* and *SOC1* floral integrators (Ratcliffe *et al.*, 2003) were highly increased in *clf-2*, *SOC1* appeared more up-regulated than *FT* in the two H3.3^{K27A} lines. This latest observation indicates that, comparatively to *clf-2*, early flowering of the H3.3^{K27A} lines is associated more with *SOC1* than with *FT* up-regulation. Together, our data point towards multiple similarities between the H3.3^{K27A} lines and the PRC2 HMT mutant *clf-2* in the regulation of flowering genes, yet with some divergences.

Besides being a flowering inducer (Lee *et al.*, 2008), *SOC1* is also necessary to limit premature floral meristem differentiation (Lee & Lee, 2010) and cambium activity (Rahimi *et al.*, 2022). Interestingly, *SOC1* remains upregulated in the H3.3^{K27A} lines after flowering inducing molecular events have taken place, that is, in 10-d-old plants (Fig. S5a). Therefore, to assess organogenesis from the shoot apex, the number of flowers produced by the primary inflorescence and the meristem size, two negatively correlated features (Landrein *et al.*, 2015), were measured. While a slight trend towards slower plastochrone could be observed in the H3.3^{K27A} lines (Figs 1e, S6), the plants displayed similar meristem radius and number of side branches as the WT control. This indicates that shorter stem length of the H3.3^{K27A} lines is not due to early meristem termination nor loss of apical dominance (Figs 1f, S6).

Finally, the H3.3^{K27A} lines showed higher proliferation rate and mass accumulation upon culturing on callus-inducing media (Fig. 1h). Since the calli derived from the PRC2 mutant *emf2* display impaired capacity to regenerate shoot (Mandel *et al.*, 2022), we also assessed this capacity, by culturing 30-d-old H3.3^{K27A} calli on SIM. After 9 d of incubation, the control H3.3 line showed dark green foci characteristic of *de novo* shoot organogenesis initials, whereas many root hairs appeared on H3.3^{K27A} line calli. After 28 d of incubation on SIM, the control H3.3 calli regenerated four to eight shoots, whereas the H3.3^{K27A} line calli failed to regenerate functional shoots (Figs 1i, S7). Instead, the calli developed aberrant structures, reminiscent of the PRC2 *clf swn* double mutant (Chanvivattana *et al.*, 2004).

Cell fates are affected in stems of the H3.3^{K27A} lines

The short-stemmed H3.3^{K27A} plants also displayed morphologic defects at the epidermis. Indeed, SEM analysis on stems revealed cells with aberrant shapes, as well as wrong positioning and

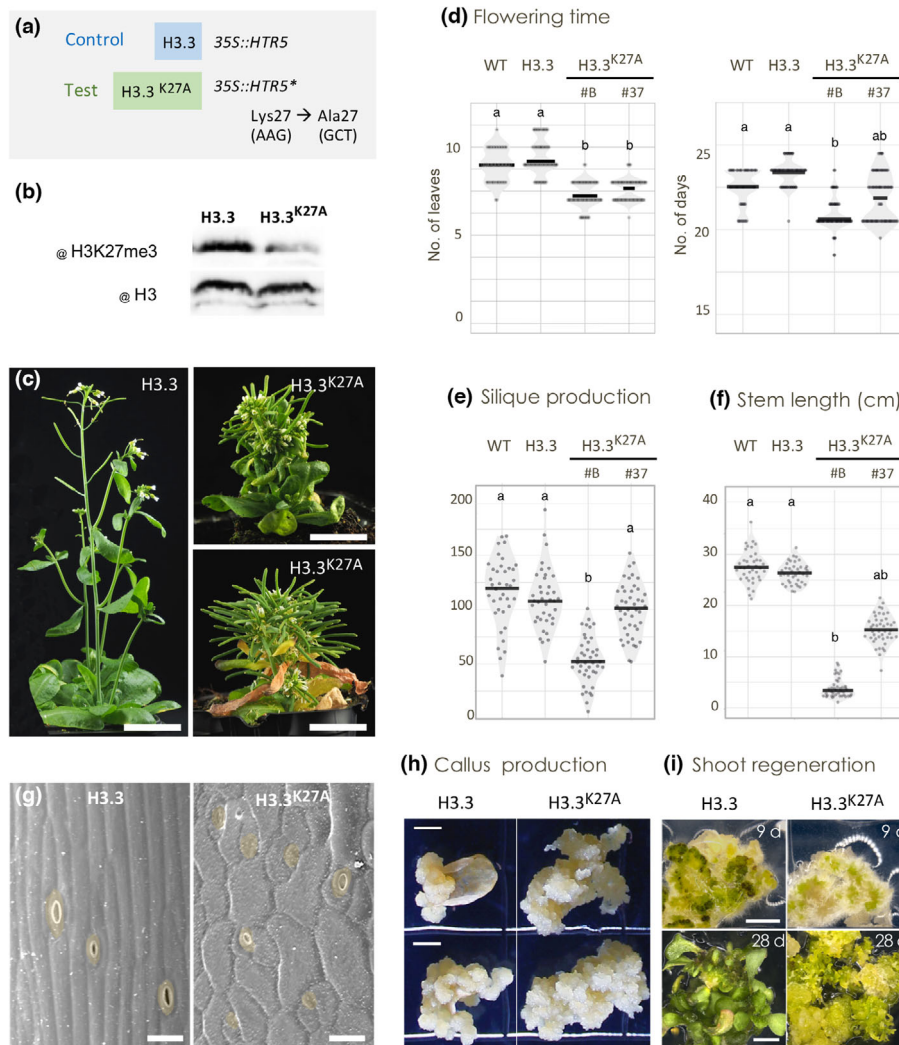
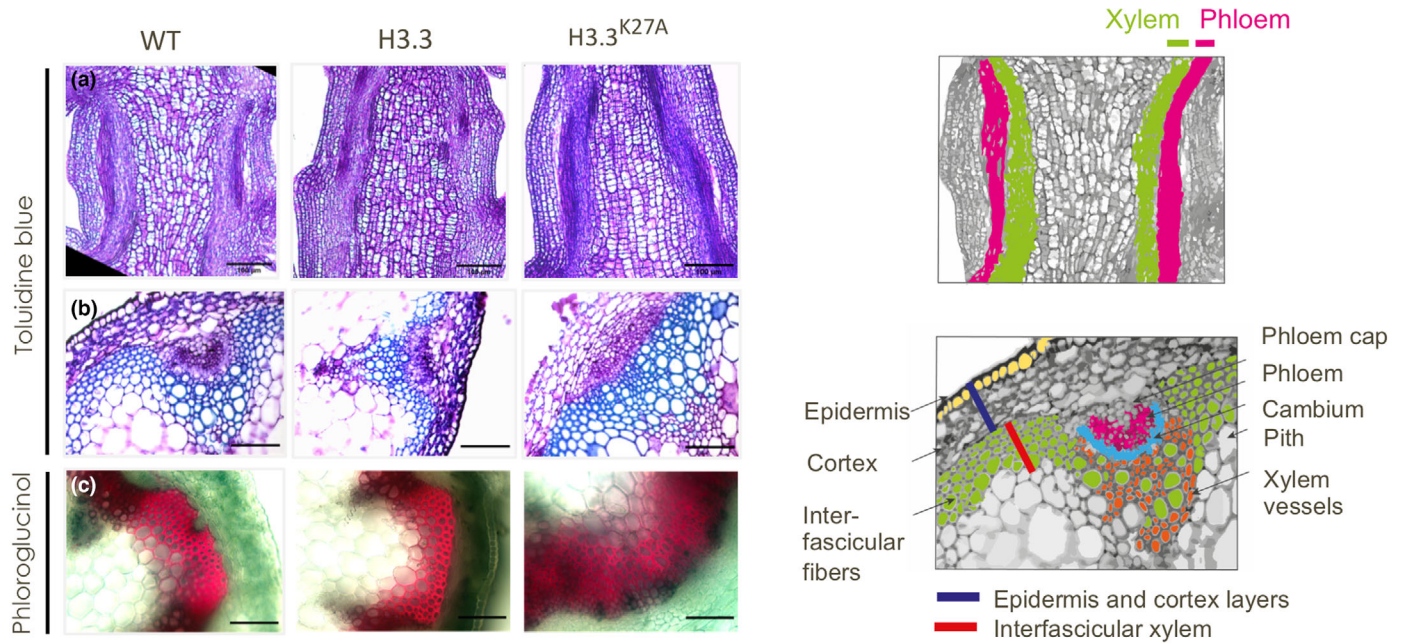


Fig. 1 Overview of the alterations in developmental transitions displayed by the *Arabidopsis thaliana* plants expressing H3.3^{K27A}: leaf morphology, stem morphology and elongation, flowering transition, flower production, enhanced callus production and impaired shoot regeneration. (a) Schematic illustration of the transgenic constructs used to produce the control (H3.3) and test (H3.3^{K27A}) lines in the Landsberg erecta (Ler) ecotype. (b) Western blot analysis of total H3 accumulation and H3K27me3 level in control H3.3- and H3.3^{K27A}-expressing plants. (c) Representative images of the adult plant phenotypes from the H3.3 and H3.3^{K27A} lines. Side views of plants at 45 or 60 (right-lower panel) d post-germination. Bars, 3 cm. (d) Flowering time, scored by number of leaves (left) and number of days (right) at bolting. Plots illustrating the data on the flowering time of the WT, H3.3 and two independent lines of H3.3^{K27A} plants ($n = 57, 80, 84$ and 87 for WT, H3.3, H3.3^{K27A} #B and H3.3^{K27A} #37, respectively). (e) Total number of siliques produced on the main stem ($n = 38, 39, 42$ and 44 for WT, H3.3, H3.3^{K27A} #B and H3.3^{K27A} #37, respectively). (f) Main inflorescence stem length, in cm ($n = 38, 39, 42$ and 44 for WT, H3.3, H3.3^{K27A} #B and H3.3^{K27A} #37, respectively). Black lines in d to f represent the median and the dots values of individual samples; the samples are assembled in statistical groups by the P -values of Tukey pairwise comparison test. In panels (d–f), letters indicate significant differences (Student's t -test with Benjamini–Hochberg FDR correction, P -value < 0.05). All plants were grown under LD (16 h : 8 h) at 21°C. Data were collected from three independently grown plant populations. (g) Scanning electron microscopy images of inflorescence stem surfaces of 32-d old plants of H3.3 and H3.3^{K27A} genotypes. Stomata cells or founder cells are colored in yellow. Bars, 25 μ m. (h) Callus production from leaves 3 and 4 taken from H3.3 and H3.3^{K27A} seedlings and incubated on callus-inducing media (CIM) for 30 d. Bars, 200 μ m. (i) H3.3 and H3.3^{K27A} 30-d-old calli were transferred to shoot-inducing media (SIM) and images were taken after 9 and 28 d of incubation under light. Bars, 200 μ m.

spacing of stomata initiator cells and incomplete differentiation of stomata from meristemoid mother cells (Figs 1g, S8). To further characterize morphological defects at inflorescence stems, we performed in-depth histological analyses on stem longitudinal and cross sections. We found that the cell-type distribution is affected in H3.3^{K27A} stems (Fig. 2a–c). In particular, toluidine blue and phloroglucinol staining of the tissue sections revealed a thickening of the lignified tissue layers with a wide range of increase, from 50% to 100% as compared to the H3.3 control,

and an irregularity in the distribution of vascular bundles (Figs 2d, S9). Further quantification showed that thickening of the interfascicular cambium-derived tissues was preferentially due to a significant increase in cell layer number than changes in cell sizes (Figs 2d, S9, S10). At the same time, the thickness of the phloem layer within the vasculature bundles appeared unchanged in H3.3^{K27A} stems (Fig. S10). Finally, a tendency for epidermis and cortex layer thickening was also observed in H3.3^{K27A} stems (Fig. S10). These defects, while observed in both analysed



(d) Intervascular xylem (lower stem sections)

No. of cell layers

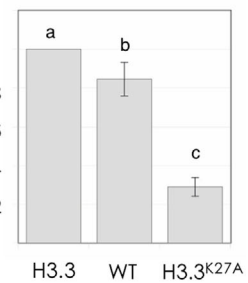
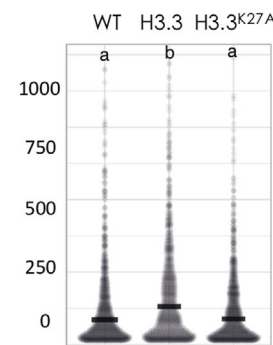
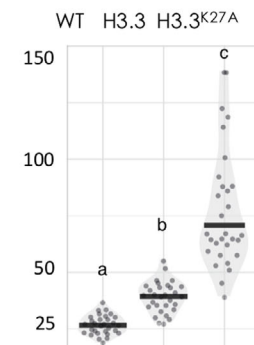
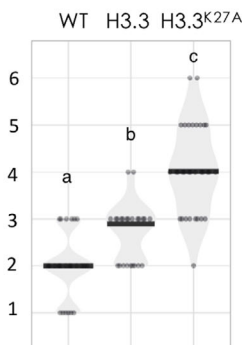
Thickness of tissue (μm)Lignified cell area (UN)
[Phloroglucinol stain](e) *WOX4* expression
in lower stems
(fold-change)

Fig. 2 Differentiation of cell layers is affected in stems of the H3.3^{K27A} lines. (a, b) Representative images of longitudinal (a) and transversal (b) microtome sections of paraplast-embedded tissues from the base of the main inflorescence stem of WT, H3.3 and H3.3^{K27A} plants, stained with Toluidine blue. (c) Representative images of transversal free hand sections of lower inflorescence stems from H3.3 and H3.3^{K27A} plants (0.7–1 cm above the rosette and under the first side branch, 2.5 wk after bolting), stained with Phloroglucinol-HCl. Bars, 100 μm . The right panel represents the schematic drawing of the longitudinal (a) and transversal (b) sections of the inflorescence stems with the tissues (colour code) and regions taken to measure layer thickness. Bars, 100 μm . (d) Plots illustrating the measurements of the number of cell layers (left panel, $n = 24$, 24 and 32 for WT, H3.3 and H3.3^{K27A}, respectively); thickness of tissue (centre, $n = 30$ for all genotypes); areas of lignified cells (right, $n = 1000$ cells for all genotypes). In panels (d) and (e), letters indicate assembly of samples in statistical groups by the P -values of Tukey pairwise comparison test ($P < 0.05$). Circles represent values for individual samples, the whiskers span from the minimum to the maximum value, and the horizontal line represent the median. (e) Histogram illustrating the abundance of the *WOX4* transcript in the base parts of inflorescence stems of the H3.3, WT and H3.3^{K27A} plants, as measured by RT-qPCR. Data were normalized to *TUB4* and presented relative to H3.3 (set as 1). Error bars represent the standard deviation of the three technical repeats, from one representative biological repeat; in panels (d) and (e), letters indicate assembly of samples in statistical groups by the P -values of Tukey pairwise comparison test ($P < 0.05$). Transgenic lines shown are H3.3 #C and H3.3^{K27A} #B.

transgenic lines, were more dramatic in the globally more affected line #B (Figs 2, S9, S10), once again revealing a positive correlation between strength of phenotypes within a same line. Interestingly, we found that the expression level of the TF *WUSCHEL*-related *HOMEBOX4* (*WOX4*), an important regulator of cambium cell division and maintenance of the vascular meristem

organization during secondary growth (Hirakawa *et al.*, 2010), was reduced in the stems of H3.3^{K27A} plants (Fig. 2e). A decrease in *WOX4* expression is known to promote xylem differentiation (Hu *et al.*, 2022), as observed in the stems of H3.3^{K27A} lines.

In summary, the lysine 27 of H3.3 plays an important role in leaf morphology, stem elongation, floral transition and *de novo*

organogenesis. Moreover, the H3.3^{K27A} lines display phenotypes never reported for the PRC2 mutants, thus revealing novel functions.

The global level of H3K27me₃, but not H3K27me₁ is clearly reduced in H3.3^{K27A}-expressing lines

Next, we analysed the histone mark contents of the H3.3^{K27A} lines by western blot analyses, which revealed a decrease in H3K27me₃ (Figs S2d, S11). This H3.3^{K27A} variant-induced decrease reached a level similar to that observed in the *clf* mutant (Figs S2d, S11). Interestingly, the level of H3K27me₁, a typical mark of constitutive heterochromatin, appeared unchanged in the H3.3^{K27A} lines, suggesting a H3 variant sorting for the mono-methylation of K27. This is in agreement with the report that H3.1, rather than H3.3, carries the H3K27me₁ mark (Sequeira-Mendes *et al.*, 2014). In addition, while *clf-2* loss-of-function causes an increase in the level of H3K27 acetylation, this is not the case for the H3.3^{K27A} lines, in which a slight decrease in H3K27ac is observed, likely due to the presence of H3.3K27A that is not modifiable by any enzyme targeting K27. Finally, the opposite effect on the H3K4me₃ mark observed in the *clf-2* mutant background was not observed in the H3.3^{K27A} lines, reinforcing the advantage of our approach for studying the genuine function of K27 and associated marks, and avoid collateral effects of the loss of PRC2 activity (Fig. S11).

RNA-seq and ChIP-qPCR on H3K27me₃ reveal the effects of the H3.3^{K27A} mutation on gene-specific transcriptional regulators and metabolite interconversion enzymes

To study the effect of H3K27A on gene expression, we performed mRNA-seq analysis on 30-d-old calli generated from the H3.3 (#C) control and H3.3^{K27A} (#B) lines. Using calli allowed us to compare cells of similar identity, thereby limiting the eventual bias induced by comparing organs of different developmental stages and/or morphologies.

First, we found by PCA of gene expression that the H3.3^{K27A} line clearly separated from the rather overlapped WT and H3.3 controls (Fig. S12). In addition, more genes were found to be up-regulated (1764, log₂FC ≥ 1) than down-regulated (1337, log₂FC ≤ -1) in calli-expressing H3.3^{K27A} as compared to those expressing the control H3.3 (Fig. 3a; Table S2).

Out of the 1764 up-regulated genes in H3.3^{K27A}, 534 (30%) were identified as H3K27me₃-marked genes in WT calli grown under the same conditions (Mandel *et al.*, 2022; representation factor (RF) = 2.1, *P*-value < 8.495e-71 for significant overlap). The up-regulation of these 534 genes is therefore likely a direct consequence of the K27A substitution and the resulting decrease in H3K27me₃ (Fig. 3b; Table S3). Furthermore, among the 534 genes up-regulated in H3.3^{K27A}, only 195 are part of the 370 *emf2* up-regulated genes (compared with WT, log₂FC ≥ 1; Mandel *et al.*, 2022). This indicates that our approach results in a widespread H3K27me₃ decrease that goes beyond that of the PRC2 mutant *emf2*, whose smaller population of mis-regulated genes likely reflects redundancy between PRC2 components.

Gene ontology analyses on the 1764 up-regulated genes in H3.3^{K27A} (log₂FC ≥ 1) revealed a large proportion of metabolite interconversion enzymes (42.3%) and gene-specific transcriptional regulators (15.6%; Fig. 3d). Altogether, there are 213 TF-encoding genes up-regulated in H3.3^{K27A}, with a majority of helix-turn-helix (HTH), MADS and basic helix-loop-helix (bHLH) encoding genes (Fig. 3d). Interestingly, the proportion of TF-encoding genes increases among the H3.3^{K27A} up-regulated genes covered by H3K27me₃ in WT callus (Figs 3f, S13). This proportion further increases when considering the 109 genes that are also up-regulated in the *emf2* mutant (Figs 3d, S13), especially for MADS genes (from 26.9% to 41.2%).

Remarkably, out of the 431 *emf2* down-regulated genes (log₂FC ≤ -1), 146 are also down-regulated in H3.3^{K27A}, (Fig. 3c; Table S4) which corresponds to a significant overlap in target lists (RF = 6.9, *P*-value < 8.891e-83). Because this population of 146 genes, as well as the population of 1337 genes down-regulated in H3.3^{K27A}, is independent of the population of H3K27me₃ targets (Fig. 3c; Table S4), they likely correspond to secondary targets affected by the up-regulation of PRC2 direct targets identified in both *emf2* and H3.3^{K27A} lines. The 1337 down-regulated genes in H3.3^{K27A} are again mainly enriched in metabolites interconversion enzymes (44.8%) and gene-specific transcriptional regulators (11.7%). Among the 112 TF-encoding genes that are down-regulated in H3.3^{K27A}, 75% belong to the HTH and bHLH families (Fig. 3e), only one gene belongs to the MICK-type MADS box family and 22 to the ERF family (compared with 21 and 6, respectively, in the up-regulated genes; Figs 3e, S14; Table S4).

Interestingly, we found that *SOC1* is highly up-regulated in H3.3^{K27A} calli (log₂FC = 2.95; Table S2). This is consistent with the RT-qPCR analyses performed on seedlings (Fig. S5a) and further validates our RNA-seq approach on calli. Supporting its transcriptional down-regulation, we found by ChIP-qPCR that the amount of the H3K27me₃ mark at *SOC1* is significantly reduced in seedlings of both tested H3.3^{K27A} lines compared to the control H3.3 line (Fig. S5b). We also assessed the expression and presence of the H3K27me₃ mark at the flowering regulators *AGL24* (Lee *et al.*, 2008) and *AGL44* (Pajoro *et al.*, 2014), both highly up-regulated in H3.3^{K27A} calli (log₂FC = 2.8 and log₂FC = 2.57, respectively), and found the same trend as for *SOC1* in seedlings of the H3.3^{K27A} lines: increase in expression and consistent decrease in H3K27me₃ mark amounts (Fig. S5c–f). Interestingly, *AGL24* and *AGL44* were also reported to regulate vasculature development (Collum *et al.*, 2019; J. Zhang *et al.*, 2019).

While searching for other mis-regulated genes in the H3.3^{K27A} lines, which may be associated with the stem morphology phenotypes, we found *WRKY13* (up-regulated, log₂FC = 5.22), previously reported as required for the development of sclerenchyma cells (Table S3). Coherently, the *wrky13* mutant phenotype is opposite to that of the H3.3^{K27A} lines (Li *et al.*, 2015). Also related to this phenotype, a considerable proportion of genes mis-regulated in H3.3^{K27A} is associated with metabolic pathways involved in cell wall formation and lignification (Figs 3d,e, 4d; Tables S2, S5), indicating further links with the H3.3^{K27A} stem

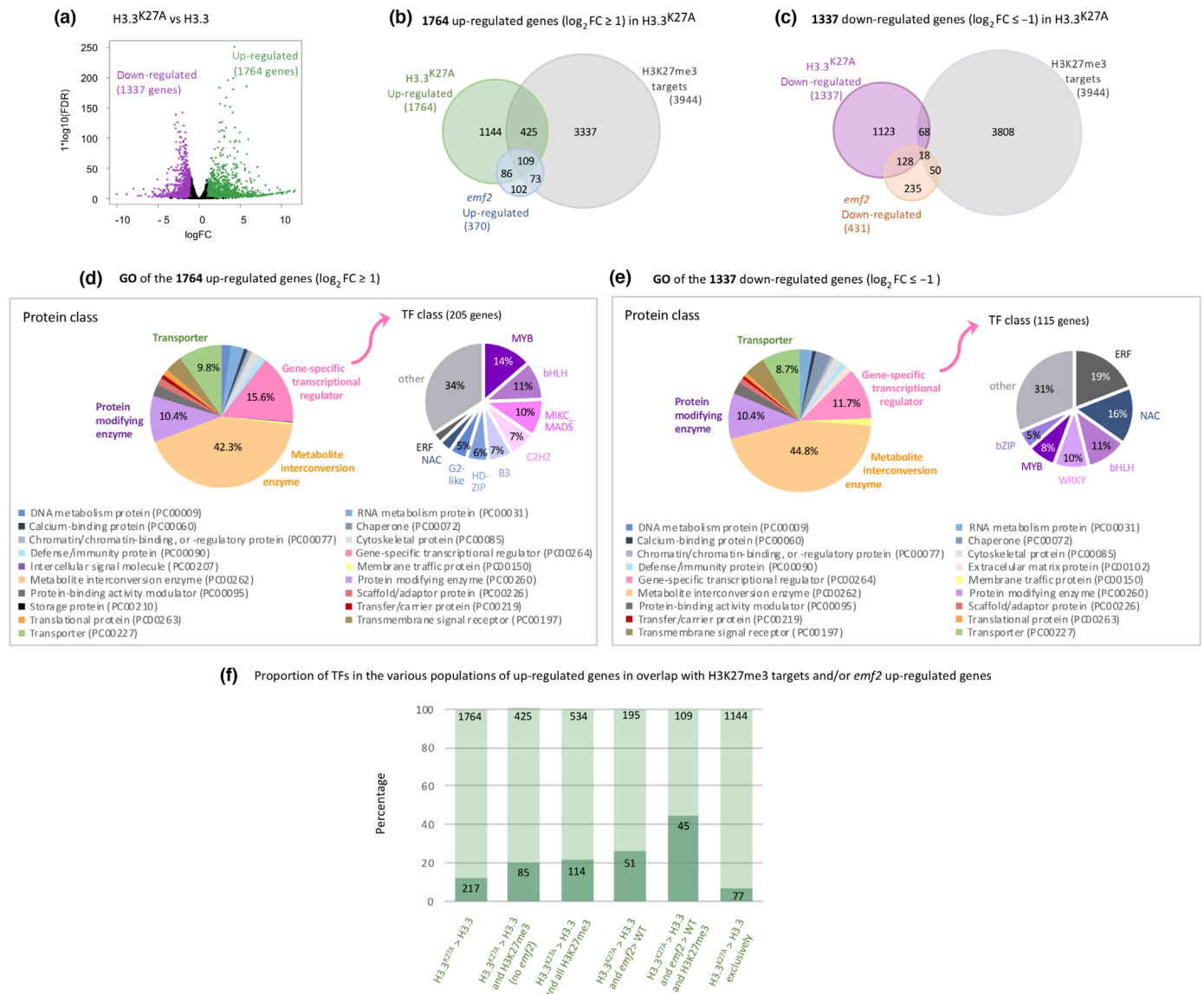


Fig. 3 Transcriptomics of the H3.3^{K27A} lines reveal a subset of up-regulated genes larger than that of down-regulated genes, with enrichment in metabolite reconversion enzymes and gene-specific transcriptional regulators. Data analysis of RNA-seq on calli from H3.3^{K27A} #B compared to H3.3 #C. While 1337 genes are down-regulated ($\log_2\text{FC} \leq -1$ and $\text{FDR} < 0.05$), 1764 are up-regulated in H3.3^{K27A} ($\log_2\text{FC} \geq 1$ and $\text{FDR} < 0.05$). (b, c) Venn diagrams for overlaps between H3.3^{K27A} mis-regulated genes and H3K27me3 targets and/or *emf2* mis-regulated genes. The full list of corresponding genes can be found in the Supporting Information Table S2. (d, e) GO analysis of the genes mis-regulated in H3.3^{K27A}, and enrichment in transcription factor (TF) classes (P -value < 0.05). (f) percentage of TFs in the various populations of up-regulated genes in overlap with H3K27me3 targets and/or *emf2* up-regulated genes. The full list of corresponding genes is found in Table S3.

phenotype. Among them are genes encoding for callose synthase-like protein (At2g30680, $\log_2\text{FC} = 9.61$), cellulose synthase-like B1 (At2g32610, $\log_2\text{FC} = 6.17$), flavonol synthases (up to $\log_2\text{FC} = 8.36$) and peroxidases (expression changes raise up to $\log_2\text{FC} = 7.43$) and ferulic acid 5-hydroxylase 1 (At4g36220, $\log_2\text{FC} = 1.99$; Table S2). In addition, several TF-encoding genes involved in the regulation of xylem development are associated with H3K27me3-enriched regions, including the bHLH protein *TARGET OF MONOPTEROS5* (*TMO5*) and NAC-domain proteins such as members of the *VASCULAR RELATED NAC DOMAIN* (*VND*) group (Hussey *et al.*, 2017). These TFs are positive regulators of secondary cell wall formation (Kubo

et al., 2005; Ohashi-Ito *et al.*, 2010; Yamaguchi *et al.*, 2011; Taylor-Teeple *et al.*, 2015). In particular, overexpression of *VND4* causes ectopic secondary cell wall growth (Zhou *et al.*, 2014). Coherently with the H3.3^{K27A} stem phenotype, the expression of *VND4* (AT1G12260, $\log_2\text{FC} = 2.32$) and *TMO5* (AT3G25710, $\log_2\text{FC} = 3.01$) is up-regulated, while that of *WOX4* is down-regulated ($\log_2\text{FC} = -1.5$) in H3.3^{K27A} (Tables S2–S4). Finally, with RT-qPCR and CHIP-qPCR experiments on H3.3^{K27A} seedlings, we could confirm the up-regulation of *TMO5* and *AT2G30680*, two genes that are targets of the H3K27me3 mark, and could correlate their mis-expression with a decrease in H3K27me3 at their loci (Fig. S15a–d).

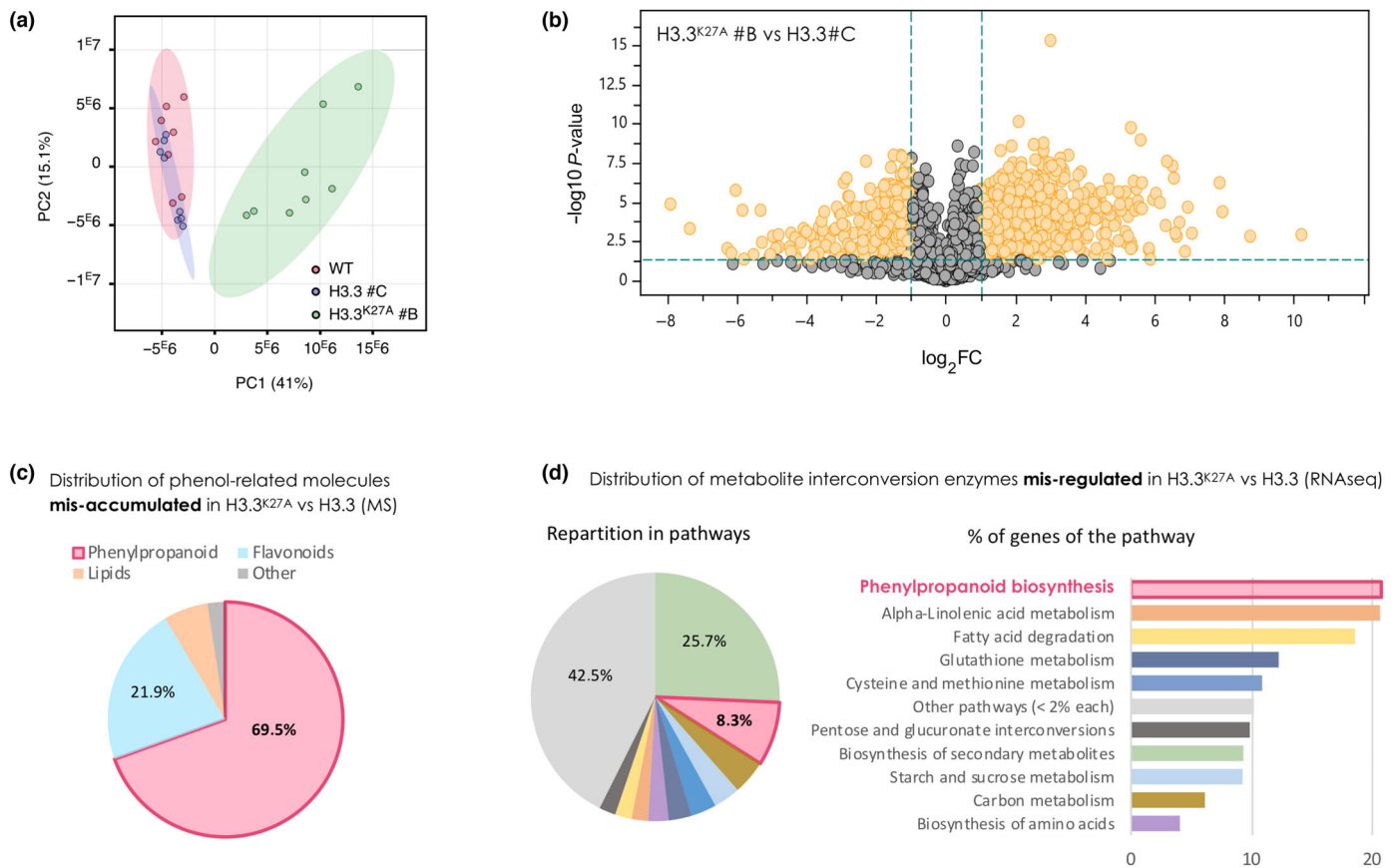


Fig. 4 Metabolomics analyses on H3.3^{K27A} lines and correlation with the transcriptomics for interconversion enzymes. (a) 2-D score plot for principal component analysis (PCA) and (b) Volcano plot showing the differential enrichment of metabolites between WT, H3.3 #C and H3.3^{K27A} #B. Each point of the PCA represents a metabolite profile of an individual biological replicate. The PCA score plot was constructed using METABOANALYST 4.0. Data were analysed by range scaling. Each point in the volcano plot represents a metabolite (or bucket). Significant buckets were calculated with a fold change (FC) threshold of ± 2 and a P -value < 0.05 (indicated in orange). The distinct separation of H3.3^{K27A} #B in both (a, b) indicates the significant enrichment/depletion of more metabolites than in H3.3 #C compared to WT. (c) Pie chart illustrating the distribution of phenol-related molecules identified from our metabolomic data to be mis-accumulated in H3.3^{K27A} as compared to H3.3 and mapped to the KEGG compounds database. (d) Pie and bar charts illustrating the distribution of the 604 genes encoding for metabolite interconversion enzymes that were identified from our RNA-seq data to be mis-regulated in H3.3^{K27A} as compared to H3.3.

In summary, for several genes involved in regulating the flowering transition, floral organ development and stem morphology, we were able to confirm that their up-regulation revealed by our RNA-seq approach on calli can also be observed in the tissues relevant for the phenotypic defects of the H3.3^{K27A} lines. Further supporting the up-regulation of these genes, we were also able to detect the decreased abundance of the repressive histone mark H3K27me3 at their chromatin regions.

Metabolomics and transcriptomics highlight a function for H3.3K27 in phenylpropanoid biosynthesis

Because the largest proportion of genes mis-regulated in H3.3^{K27A} encode for metabolic interconversion enzymes (Fig. 3; Tables S2, S5), we launched an *in situ* metabolomic investigation of the H3.3^{K27A} lines. We determined the metabolome of WT, H3.3 (#C) and H3.3^{K27A} (#B) lines through a non-targeted approach in which buckets made of a mass/charge ratio and a

retention time were used to describe molecules of interest. First, a PCA indicated a clear separate clustering for H3.3^{K27A}, while WT and H3.3 overlapped (Figs 4a, S16a). In agreement with the PCA, significantly more metabolites were found differently enriched in H3.3^{K27A} than in H3.3, compared to WT (i.e. fold change $> \pm 2$ and P -value < 0.05 ; Figs 4b, S16).

Then, an in-depth analysis of mis-accumulated phenol-related molecules revealed a great enrichment in phenylpropanoids, which are core components of lignin (Fig. 4c; Tables S5–S7). Interestingly, when returning to our RNA-seq data and detailing the pathways for metabolite interconversion enzyme-coding genes, we found a significant enrichment of genes involved in phenylpropanoid biosynthesis (Figs 4d, 5; Table S2). Strikingly, over 20% of genes of this GO pathway are mis-regulated (up- or down) in H3.3^{K27A}. More precisely, we detected a decreased expression for several genes encoding enzymes of the lignin biosynthesis pathway, such as phenylalanine ammonia-lyase (PAL1, AT2G37040, log₂FC = -1.67), cinnamic acid 4-

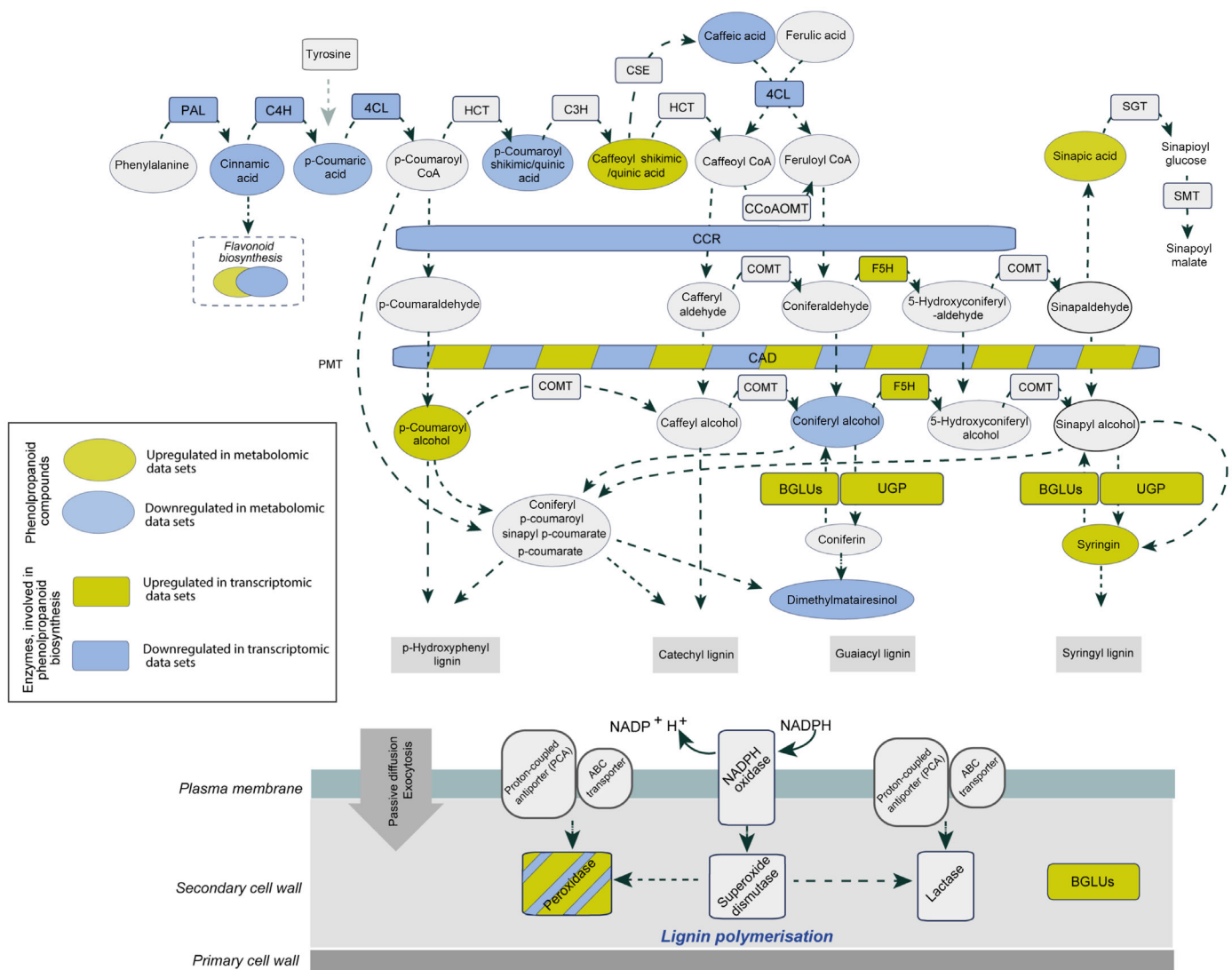


Fig. 5 Phenylpropanoid biosynthesis pathway with transcriptome and metabolome for H3.3^{K27A} vs H3.3. Representation of transcriptomics and metabolomics data for phenylpropanoid biosynthesis (H3.3^{K27A} vs H3.3). Schematic illustration, depicting the elements of the phenylpropanoid biosynthesis pathways that are detected to be mis-regulated in the metabolomic (ovals) and transcriptomic (rectangles) datasets, mapped to the KEGG pathways database, with the colour code of mustard shade for up-regulated and blue for down-regulated elements. 4CL, 4-coumarate-CoA ligase; BGLU, α -glucosidases; C3H, p-coumaroyl shikimate 3'-hydroxylase; C4H, cinnamic acid 4-hydroxylase; CAD, cinnamyl alcohol dehydrogenase; CCoAOMT, caffeoyl CoA 3-O-methyltransferase; CCR, cinnamoyl-CoA reductase; COMT, caffeate/5-hydroxyferulate 3-O-methyltransferase; CSE, caffeoyl shikimate esterase; F5H, ferulate 5-hydroxylase; HCT, hydroxycinnamoyl-CoA shikimate/quinic acid hydroxycinnamoyl transferase; PAL, phenylalanine ammonia-lyase; SGT, sinapato UDP-glucose sinapoyltransferase; SMT, 1-O-sinapoyl- β -glucose : L-malate O-sinapoyltransferase; UGT, UDP-glycosyltransferase. Combined analysis of both datasets indicates the multiple levels of this pathway are affected in the H3.3^{K27A} plants with the elements shaded in other than grey corresponding to those, affected in H3.3^{K27A} vs H3.3.

hydroxylase (C4H, AT2G30490, $\log_2FC = -1.16$), 4-coumarate-CoA ligase (4CL, AT1G51680 $\log_2FC = -1.05$; Fig. 5; Table S2). These changes in expression correlate positively with the lower content of corresponding produced compounds (i.e. cinnamic and coumaric acids and their derivatives). The expression of multiple β -glucosidases (BGLUs) and UDP-glycosyltransferases (UGTs) is also affected in H3.3^{K27A} (Fig. 5, Table S2). Interestingly, BGLU45 and BGLU46 ($\log_2FC = -1.33, -2.18$ respectively), were previously shown to be involved in the hydrolysis of monolignol glucosides, the storage form of monolignols in *Arabidopsis* (Escamilla-Treviño *et al.*, 2006; Chapelle *et al.*, 2012).

In summary, we found a correlation between misrepresented metabolic compounds, corresponding mis-regulated genes and the xylem over-proliferation in stems of the H3.3^{K27A} lines.

Discussion

The H3.3^{K27A} lines reveal developmental and molecular functions for H3.3K27

The substitution of K27 into an Alanine residue in the H3.3 protein proved to be highly instrumental in discovering novel functions for the histone lysine residue in plants. It illustrates how

loss of histone modifications, independently from loss of histone-modifying enzymes, can impact biological processes such as gene expression and biosynthetic pathways. While the H3.3^{K27A} lines displayed developmental defects reminiscent of PRC2 loss-of-function, such as early flowering, leaf morphology defects and shorter stems, our approach also revealed novel developmental features. Indeed, we found that the H3.3^{K27A} lines are not affected in flower number or morphogenesis, but have apparent defects in cell morphology and elongation in the stem epidermis, combined with a modified cell layer patterning within the stem, and faster calli proliferation.

While cytological analyses did not reveal a profound impact of H3.3^{K27A} on hetero/euchromatin spatial distribution (data not shown), our molecular analyses unveiled changes in the level of euchromatin marks in the nucleus. Indeed, while the H3.3^{K27A} variant led to a decreased loading of the H3K27me3 and H3K27ac euchromatic histone marks, it did not impact the level of the constitutive heterochromatin H3K27me1 mark, likely correlating with the globally maintained nuclear and chromatin organization in the H3.3^{K27A} lines. In *A. thaliana*, the preferred substrate of the H3K27 monomethylases ATXR5 and ATRX6 (Jacob *et al.*, 2009), which are unique to plants, was reported to be the H3.1 variant (Bieluszewski *et al.*, 2021). *In vitro* work showed that the preference of ATRX5/6 for H3.1 over H3.3 is due to a single amino acid difference at position 31 of H3, with alanine promoting H3.1 methylation, while threonine in H3.3 blocks methylation (Jacob *et al.*, 2014). Here we thus provide an *in vivo* evidence for the preferential K27 mono-methylation of H3.1 vs H3.3, indicating an efficient H3 variant sorting for the deposition of this mark.

H3.1 and H3.3 variants differ in only four amino acids, yet they have distinct deposition patterns within the chromatin, where they exert different functions (Shi *et al.*, 2011; Probst *et al.*, 2020). While H3.1, which is rather enriched at silent regions and predominantly expressed and incorporated during the S-phase, H3.3 is expressed and deposited throughout the cell cycle, independently from DNA replication (Ahmad & Henikoff, 2002; Jiang & Berger, 2017a).

Interestingly, our data also indicate that in Arabidopsis, the overexpression of canonical histones such as H3.3 has no effect on the plant growth and development (i.e. the H3.3 control lines have a WT phenotype), while this is not the case in yeast (Singh *et al.*, 2010). Another interesting point is the robustness of the observed phenotypes, for their types and strength, over generations and between individuals of a same line. This high penetrance indicates that either H3.3^{K27A} and H3.3 histones are consistently loaded at individual chromatin positions and/or that the regulation of some genes and corresponding pathways is more sensitive than others to the H3.3^{K27A}-mutated histone.

The H3K27me3 mark has been extensively reported as contributing to the maintenance of epigenetic states for expression programme memory over cell cycles in animals and plants (Mozgova *et al.*, 2015; Hugues *et al.*, 2020), rather than initiating gene expression changes (Lafos *et al.*, 2011; Engelhorn *et al.*, 2017). The developmental phenotypes observed in H3.3^{K27A} lines, including early flowering and stem cell fate defects, likely reveal a

role for H3.3K27 in establishing the regulation of target genes to be switched for a developmental transition, rather than in maintaining an already established gene expression state, hence corresponding cell fate. Overexpression of H3.3^{K27A} may mostly impact the initial deposition of repressive H3K27me3 for gene expression reprogramming, before replacement by the replication-coupled H3.1 for establishment of a maintained repressed state over cell divisions (Jiang & Berger, 2017b).

Mutating H3.3 therefore offers an experimental advantage for depicting the specific function of a histone variant, while ‘killing’ histone modifications in a variant-selective manner. As a matter of fact, H3.3^{K27A} variants, but not H3.1^{K27A} variants, induced striking developmental phenotypes in *A. thaliana* plants (data not shown).

H3.3K27 controls the capacity to regenerate tissues

Culturing H3.3^{K27A} leaves on CIM, which contains two hormones providing a strong signal to divide, resulted in faster callus formation than for the controls. Enhanced callus formation was also observed in plants overexpressing the atypical H3.15 variant lacking lysines at positions 4 (N4 instead) and 27 (H27 instead; Yan *et al.*, 2020). Authors speculated that up-regulation of *WOX11* and *LATERAL ORGAN BOUNDARIES DOMAIN18* (*LBD18*) genes promoted the callus formation. In line with the highly proliferating callus phenotype, two of the four LBD TFs (LBD16 to 18, and LBD29) that were identified as enhancers of callus formation (Fan *et al.*, 2012) are marked by H3K27me3 in WT callus and are up-regulated in H3.3^{K27A} (*LBD29*, log₂FC = 7.4; *LBD17*, log₂FC = 1.4). Previously, the up-regulation of *LBD29* in *myb94myb96* double mutant was shown to stimulate cell proliferation on CIM (Dai *et al.*, 2020). Moreover, the bZIP59–LBD complex downstream gene *FAD-binding Berberine* (*FAD-BD*), which contributes to callus formation (Xu *et al.*, 2018), is also up-regulated in H3.3^{K27A} (log₂FC = 3.8). Altogether, the callus phenotype of H3.3^{K27A} highlights the role of H3.3K27 in controlling cell proliferation on CIM.

Our H3.3^{K27A} lines reveal another, newly discovered, cell fate property: the failure to regenerate shoots from calli transferred to SIM. Indeed, H3.3^{K27A} calli grown on SIM regenerate structures reminiscent of *clfsun* double mutants (Chanvivattana *et al.*, 2004), thus establishing a link between the impaired regenerative capacity of H3.3^{K27A} and the decrease in H3K27me3. The acquisition of new fate upon regenerative stimulus requires the establishment of specific gene expression patterns, which involves mechanisms to silence the previous cell identity genes and reinforce lineage commitment (Eshed Williams, 2021). In the H3.3^{K27A} up-regulated genes, we identified many developmental TFs from different pathways, some of them being sufficient for direct differentiation and organogenesis. Among these are members of the MIKC₂-MADS or YABBY TF families, which corresponding genes are marked by H3K27me3 in WT callus. We thus propose that the failure of H3.3^{K27A} calli to regenerate shoot is due to a lack of silencing of these TF-encoding genes to allow the shoot programme to dominate.

H3.3K27 is a critical epigenetic checkpoint for stem morphogenesis and lignin biosynthesis

With an integrative approach gathering transcriptomics and metabolomics, we found a correlation between mis-regulated genes and mis-represented metabolites, in connection with some of the H3.3^{K27A} phenotypes. Indeed, short-stemmed H3.3^{K27A} plants displayed morphologic defects both at the epidermis and the inner stem cell layers. In particular, histological analyses on stem longitudinal and cross sections revealed thickening of the lignified tissues layers and vasculature bundles, indicating mis-regulation of cell specification. Interestingly, we found that the expression of several genes involved in the regulation of this process is affected in H3.3^{K27A} plants. Among them are *WOX4* (AT1G46480 log₂FC = -1.5) and *ATHB8* (AT4G32880 log₂FC = -0.75), both known to initiate the self-division of cambium cells, thereby controlling vascular cell proliferation and secondary growth of the stem both in Arabidopsis and Poplar (Hirakawa *et al.*, 2010; Kucukoglu *et al.*, 2017). A decrease in *WOX4* expression was reported to correlate with the elevated expression of *MONOPTEROS (MP)* in a module regulating wood formation (Brackmann *et al.*, 2018). While the expression of *MP* did not seem to be significantly affected in H3.3^{K27A} seedlings, we detected that *TMO5* (AT3G25710) is up-regulated, with a coherent level decrease in the H3K27me3 mark amount at its chromatin region. We observed the same trend for other genes contributing to vasculature development: *AGL24* (J. Zhang *et al.*, 2019), *AGL44* (Collum *et al.*, 2019) and *AT2G30680* (encoding for a callose synthase-like protein). Together, our dataset indicates towards a multi-level mis-regulation of the cell-lineage specification in H3.3^{K27A} plants, and the vulnerability of the vasculature development regulation towards the changes in K27 on H3.3.

Finally, the fact that many genes involved in multiple biosynthetic pathways were found mis-regulated in H3.3^{K27A} prompted us to explore its metabolome. Metabolomics is a powerful approach to explore how genetic diversity may affect phenotypic variations in plants, but was until now never used in the context of chromatin. It revealed a mis-accumulation of phenol-related molecules, among which phenylpropanoid components were the most represented, thus confirming the effect of the identified transcriptomic mis-regulation on the production of plant metabolic components.

Transcriptomics data reveal overlap and differences between H3.3^{K27A} and *emf2* PRC2 mutant lines

The role of H3.3K27 is revealed by the mis-regulation of > 3000 genes, out of which > 1700 are up-regulated, and 620 (> 36%) are direct targets of H3K27me3 or of PRC2. In general, studies on PRC2 mutants such as *clf*, *swn* or *emf2* do not show such a good overlap even when considering PRC2-bound genes (Shu *et al.*, 2019; Mandel *et al.*, 2022). Comparing our RNA-seq data with dataset obtained on *emf2* calli, we found that there are many more up-regulated genes in the H3.3^{K27A} calli than in the PRC2 loss-of-function mutant. Among the TF families up-regulated in

H3.3^{K27A}, whose proportion increases when looking at genes covered with H3K27me3 and up-regulated in *emf2*, the fraction of MADS-encoding genes increases the most. This is in agreement with the many reports showing that MADS TFs are key targets for PRC2 regulation (Kim *et al.*, 2012; Engelhorn *et al.*, 2017; Zhang *et al.*, 2018). Interestingly and differently to the TF-encoding genes up-regulated in H3.3^{K27A}, most of the down-regulated TF-encoding genes also known to be H3K27me3 targets, encode for HTH and bHLH families only.

Our approach using the non-methylable H3.3^{K27A} variant thus reveals the mis-expression of a larger set of H3K27me3-regulated genes than when using PRC2 mutants. An example illustrating this, and that we characterize in our study, is that of the *SOCI* gene that is not found among the *emf2* up-regulated genes (Mandel *et al.*, 2022), while detected as up-regulated in our study using the H3.3^{K27A} mutant instead (both from the RNA-seq, RT-qPCR and ChIP-qPCR). The H3.3^{K27A}-encoding gene is driven by a strong constitutive promoter known to conduct gene expression in most cell types of most plant organs. Therefore, in the corresponding tissues, the overexpressed histone variant has likely been integrated into the chromatin randomly, in competition with the proteins produced from the endogenous H3-encoding genes. Consequently, our approach provides an advantage over the use of mutants in mark writers that are subjected to specific tissue or vary in expression level between different cell types (de Lucas *et al.*, 2016).

In brief, our study reveals that the histone H3.3 K-to-A mutation at K27 acts as a dominant-negative gain-of-function mutation in plants. Expression of the H3.3^{K27A} variant leads to unique developmental aberrations, part of them reminiscent of PRC2 mutant phenotypes and part of them novel. They include early flowering, leaf morphology defects, impaired stem elongation and cell layer patterning. Transcriptomic and metabolomic analyses allowed us to correlate newly discovered phenotypes to defective biosynthetic pathways, in particular that of the phenylpropanoid pathway related to lignin biosynthesis. Finally, given the highly conserved H3 sequence across the plant and animal kingdom(s), mutations at K27 provide a mean to alter epigenetic landscapes in organisms where histone methyltransferases are uncharacterized or where genetic studies are challenging due to multiple redundancies and multifaceted functions.

Acknowledgements

We thank Muriel Kabus, Pauline Brun, Elda Bauda for help with plant culture and selection of transgenic lines, and Emmanuel Thévenon for synthetic DNA cloning and plasmid amplification. This work was supported by the Agence Nationale de la Recherche (ANR-18-CE20-0011-01, PRC project REWIRE to CCC, AB and MEC), the Grenoble Alliance for Cell and Structural Biology (ANR-10-LABX-49-01) and the Giant International Internship program.





Competing interests

None declared.

Author contributions

Design of the research strategy: CCC and LEW. Research experiments: KF (flowering time, organogenesis, apex and stem measurements, histology, RT-qPCR and CHIP-qPCR for stem features), MLM (genetics, genotyping and RT-PCR for selection of transgenic lines), DT (sample preparation for metabolomic work), AB (flowering time, western blots, measurements and RT-qPCR for flowering time), EP (selection and primary analyses of transgenic lines), NI (stem SEM), N-LM (callus and regeneration), CV (metabolomics), CCC (construction, selection and phenotypic analyses of transgenic lines, plant imaging, western blot). Data collection and analysis: KF (statistical analyses of phenotypes, image processing and analysis, RNA-seq analysis, metabolomics analysis), AB (RT-qPCR, RNA-seq analysis, metabolomic analysis), AF (RNA-seq collection and analysis), CV (metabolomic collection and analysis), LEW and CCC (population overlaps, enrichments and GO analyses on RNA-seq and metabolomics). Data interpretation: KF (flowering, organogenesis, stem, RT-qPCR, reconstruction of the phenylpropanoid biosynthesis pathways from transcriptomics and metabolomics), AB (flowering, RT-qPCR, RNA-seq, metabolomics), LEW (callus, stem SEM, RNA-seq) and CCC (flowering, RT-qPCR, RNA-seq, metabolomics). Funding for the study: CCC, AB, M-EC and LEW. CCC wrote the manuscript with the help of LEW, AB and KF. All authors read and approved the final manuscript.

ORCID

Alexandre Berr  <https://orcid.org/0000-0002-1381-9053>
 Cristel C. Carles  <https://orcid.org/0000-0002-9416-4860>
 Marie-Edith Chabouté  <https://orcid.org/0000-0001-8688-721X>
 Kateryna Fal  <https://orcid.org/0000-0001-5187-0290>
 Claire Villette  <https://orcid.org/0000-0003-2564-5529>
 Leor Eshed Williams  <https://orcid.org/0000-0002-2766-2608>

Data availability

Transcriptomics and metabolomics data that support the findings of this study are available as article supplementary information material (Supplementary Tables). Transcriptomics raw data that support the findings of this study are openly available in the NCBI Sequence Read Archive repository platform (SRA) at (<http://www.ncbi.nlm.nih.gov/bioproject/909476>), reference number (BioProject ID) PRJNA909476.

References

Ahmad K, Henikoff S. 2002. The histone variant H3.3 marks active chromatin by replication-independent nucleosome assembly. *Molecular Cell* 9: 1191–1200.
 Baile F, Gómez-Zambrano Á, Calonje M. 2022. Roles of Polycomb complexes in regulating gene expression and chromatin structure in plants. *Plant Communications* 3: 100267.
 Benhamed M, Bertrand C, Servet C, Zhou DX. 2006. Arabidopsis GCN5, HD1, and TAF1/HAF2 interact to regulate histone acetylation required for light-responsive gene expression. *Plant Cell* 18: 2893–2903.

Berr A, Shafiq S, Pinon V, Dong A, Shen W-H. 2015. The trxG family histone methyltransferase SET DOMAIN GROUP 26 promotes flowering *via* a distinctive genetic pathway. *The Plant Journal* 81: 316–328.
 Bertrand C, Benhamed M, Li Y-F, Ayadi M, Lemonnier G, Renou J-P, Delarue M, Zhou D-X. 2005. Arabidopsis HAF2 gene encoding TATA-binding protein (TBP)-associated factor TAF1, is required to integrate light signals to regulate gene expression and growth. *Journal of Biological Chemistry* 280: 1465–1473.
 Bertrand C, Bergounioux C, Domenichini S, Delarue M, Zhou DX. 2003. Arabidopsis histone acetyltransferase AtGCN5 regulates the floral meristem activity through the WUSCHEL/AGAMOUS pathway. *The Journal of Biological Chemistry* 278: 28246–28251.
 Besnard F, Rozier F, Vernoux T. 2014. The AHP6 cytokinin signaling inhibitor mediates an auxin-cytokinin crosstalk that regulates the timing of organ initiation at the shoot apical meristem. *Plant Signaling & Behavior* 9: e28788.
 Bieluszewski T, Xiao J, Yang Y, Wagner D. 2021. PRC2 activity, recruitment, and silencing: a comparative perspective. *Trends in Plant Science* 26: 1186–1198.
 Brackmann K, Qi J, Gebert M, Jouanet V, Schlamp T, Grünwald K, Wallner E-S, Novikova DD, Levitsky VG, Agusti J *et al.* 2018. Spatial specificity of auxin responses coordinates wood formation. *Nature Communications* 9: 875.
 Carles CC, Fletcher JC. 2009. The SAND domain protein ULTRAPETALA1 acts as a trithorax group factor to regulate cell fate in plants. *Genes & Development* 23: 2723–2728.
 Carles CC, Ha CM, Jun JH, Fiume E, Fletcher JC. 2010. Analyzing shoot apical meristem development. In: Hennig L, Köhler C, eds. *Methods in molecular biology. Plant developmental biology*. Totowa, NJ, USA: Humana Press, 105–129.
 Chan KM, Fang D, Gan H, Hashizume R, Yu C, Schroeder M, Gupta N, Mueller S, James CD, Jenkins R *et al.* 2013. The histone H3.3K27M mutation in pediatric glioma reprograms H3K27 methylation and gene expression. *Genes & Development* 27: 985–990.
 Chanvivattana Y, Bishopp A, Schubert D, Stock C, Moon Y-H, Sung ZR, Goodrich J. 2004. Interaction of Polycomb-group proteins controlling flowering in Arabidopsis. *Development* 131: 5263–5276.
 Chapelle A, Morreel K, Vanholme R, Le-Bris P, Morin H, Lapierre C, Boerjan W, Jouanin L, Demont-Caulet N. 2012. Impact of the absence of stem-specific β -glucosidases on lignin and monolignols. *Plant Physiology* 160: 1204–1217.
 Chaubet-Gigot N, Kapros T, Flenet M, Kahn K, Gigot C, Waterborg JH. 2001. Tissue-dependent enhancement of transgene expression by introns of replacement histone H3 genes of Arabidopsis. *Plant Molecular Biology* 45: 17–30.
 Clough SJ, Bent AF. 1998. Floral dip: a simplified method for *Agrobacterium*-mediated transformation of *Arabidopsis thaliana*. *The Plant Journal* 16: 735–743.
 Collum TD, Lutton E, Raines CD, Dardick C, Culver JN. 2019. Identification of phloem-associated transcriptome alterations during leaf development in *Prunus domestica* L. *Horticulture Research* 6: 16.
 Dai X, Liu N, Wang L, Li J, Zheng X, Xiang F, Liu Z. 2020. MYB94 and MYB96 additively inhibit callus formation *via* directly repressing LBD29 expression in *Arabidopsis thaliana*. *Plant Science* 293: 110323.
 Derkacheva M, Hennig L. 2014. Variations on a theme: Polycomb group proteins in plants. *Journal of Experimental Botany* 65: 2769–2784.
 Engelhorn J, Blanvillain R, Carles CC. 2014. Gene activation and cell fate control in plants: a chromatin perspective. *Cellular and Molecular Life Sciences* 71: 3119–3137.
 Engelhorn J, Blanvillain R, Kröner C, Parrinello H, Rohmer M, Posé D, Ott F, Schmid M, Carles C. 2017. Dynamics of H3K4me3 chromatin marks prevails over H3K27me3 for gene regulation during flower morphogenesis in *Arabidopsis thaliana*. *Epigenomes* 1: 8.
 Escamilla-Treviño LL, Chen W, Card ML, Shih M-C, Cheng C-L, Poulton JE. 2006. *Arabidopsis thaliana* β -glucosidases BGLU45 and BGLU46 hydrolyse monolignol glucosides. *Phytochemistry* 67: 1651–1660.
 Eshed Williams L. 2021. Genetics of shoot meristem and shoot regeneration. *Annual Review of Genetics* 55: 661–681.

- Fal K, Tomkova D, Vachon G, Chabouté M-E, Berr A, Carles CC. 2021. Chromatin manipulation and editing: challenges, new technologies and their use in plants. *International Journal of Molecular Sciences* 22: 512.
- Fan M, Xu K, Hu Y. 2012. Lateral organ boundaries domain transcription factors direct callus formation in *Arabidopsis* regeneration. *Cell Research* 22: 1169–1180.
- Fang D, Gan H, Cheng L, Lee J-H, Zhou H, Sarkaria JN, Daniels DJ, Zhang Z. 2018. H3.3K27M mutant proteins reprogram epigenome by sequestering the PRC2 complex to poised enhancers. *eLife* 7: e36696.
- Finogenova K, Bonnet J, Poepsel S, Schäfer IB, Finkl K, Schmid K, Litz C, Strauss M, Benda C, Müller J. 2020. Structural basis for PRC2 decoding of active histone methylation marks H3K36me2/3. *Biochemistry* 9: e61964.
- Gehre M, Bunina D, Sidoli S, Lübke MJ, Diaz N, Trovato M, Garcia BA, Zaugg JB, Noh K-M. 2020. Lysine 4 of histone H3.3 is required for embryonic stem cell differentiation, histone enrichment at regulatory regions and transcription accuracy. *Nature Genetics* 52: 273–282.
- Godwin J, Farrona S. 2022. The importance of networking: plant Polycomb repressive complex 2 and its interactors. *Epigenomes* 6: 8.
- Goodrich J, Puangsomlee P, Martin M, Long D, Meyerowitz EM, Coupland G. 1997. A Polycomb-group gene regulates homeotic gene expression in *Arabidopsis*. *Nature* 386: 44–51.
- Grimaud C, Negre N, Cavalli G. 2006. From genetics to epigenetics: the tale of Polycomb group and trithorax group genes. *Chromosome Research* 14: 363–375.
- Herz HM, Morgan M, Gao X, Jackson J, Rickels R, Swanson SK, Florens L, Washburn MP, Eissenberg JC, Shilatifard L. 2014. Histone H3 lysine-to-methionine mutants as a paradigm to study chromatin signaling. *Science* 345: 1065–1070.
- Hirakawa Y, Kondo Y, Fukuda H. 2010. TDIF peptide signaling regulates vascular stem cell proliferation via the *WOX4* homeobox gene in *Arabidopsis*. *Plant Cell* 22: 2618–2629.
- Hu J, Hu X, Yang Y, He C, Hu J, Wang X. 2022. Strigolactone signaling regulates cambial activity through repression of *WOX4* by transcription factor BES1. *Plant Physiology* 188: 255–267.
- Hugues A, Jacobs CS, Roudier F. 2020. Mitotic inheritance of PRC2-mediated silencing: mechanistic insights and developmental perspectives. *Frontiers in Plant Science* 11: 262.
- Hussey SG, Loots MT, van der Merwe K, Mizrachi E, Myburg AA. 2017. Integrated analysis and transcript abundance modelling of H3K4me3 and H3K27me3 in developing secondary xylem. *Scientific Reports* 7: 3370.
- Ingham PW. 1983. Differential expression of bithorax complex genes in the absence of the extra sex combs and trithorax genes. *Nature* 306: 591–593.
- Iwakawa H, Carter BC, Bishop BC, Ogas J, Gelvin SB. 2017. Perturbation of H3K27me3-associated epigenetic processes increases *Agrobacterium*-mediated transformation. *Molecular Plant–Microbe Interactions* 30: 35–44.
- Jacob Y, Bergamin E, Donoghue MT, Mongeon V, LeBlanc C, Voigt P, Underwood CJ, Brunzelle JS, Michaels SD, Reinberg D *et al.* 2014. Selective methylation of histone H3 variant H3.1 regulates heterochromatin replication. *Science* 343: 1249–1253.
- Jacob Y, Feng S, LeBlanc CA, Bernatavichute YV, Stroud H, Cokus S, Johnson LM, Pellegrini M, Jacobsen SE, Michaels SD. 2009. ATXR5 and ATXR6 are H3K27 monomethyltransferases required for chromatin structure and gene silencing. *Nature Structural & Molecular Biology* 16: 763–768.
- Jiang D, Berger F. 2017a. Histone variants in plant transcriptional regulation. *Biochimica et Biophysica Acta* 1860: 123–130.
- Jiang D, Berger F. 2017b. DNA replication-coupled histone modification maintains Polycomb gene silencing in plants. *Science* 357: 1146–1149.
- Justin N, Zhang Y, Tarricone C, Martin SR, Chen S, Underwood E, De Marco V, Haire LF, Walker PA, Reinberg D *et al.* 2016. Structural basis of oncogenic histone H3K27M inhibition of human Polycomb repressive complex 2. *Nature Communications* 7: 11316.
- Kanehisa M. 2004. The KEGG resource for deciphering the genome. *Nucleic Acids Research* 32: 277D–280D.
- Kim SY, Lee J, Eshed-Williams L, Zilberman D, Sung ZR. 2012. EMF1 and PRC2 cooperate to repress key regulators of *Arabidopsis* development. *PLoS Genetics* 8: e1002512.
- Klymenko T, Muller J. 2004. The histone methyltransferases Trithorax and Ash1 prevent transcriptional silencing by Polycomb group proteins. *EMBO Reports* 5: 373–377.
- Kubo M, Udagawa M, Nishikubo N, Horiguchi G, Yamaguchi M, Ito J, Mimura T, Fukuda H, Demura T. 2005. Transcription switches for protoxylem and metaxylem vessel formation. *Genes & Development* 19: 1855–1860.
- Kucukoglu M, Nilsson J, Zheng B, Chaabouni S, Nilsson O. 2017. *WUSCHEL*-*RELATED HOMEBOX 4* (*WOX 4*)-like genes regulate cambial cell division activity and secondary growth in *Populus* trees. *New Phytologist* 215: 642–657.
- Lafos M, Kroll P, Hohenstatt ML, Thorpe FL, Clarenz O, Schubert D. 2011. Dynamic regulation of H3K27 trimethylation during *Arabidopsis* differentiation. *PLoS Genetics* 7: e1002040.
- Landrein B, Refahi Y, Besnard F, Hervieux N, Mirabet V, Boudaoud A, Vernoux T, Hamant O. 2015. Meristem size contributes to the robustness of phyllotaxis in *Arabidopsis*. *Journal of Experimental Botany* 66: 1317–1324.
- Leatham-Jensen M, Uyehara CM, Strahl BD, Matera AG, Duronio RJ, McKay DJ. 2019. Lysine 27 of replication-independent histone H3.3 is required for Polycomb target gene silencing but not for gene activation. *PLoS Genetics* 15: e1007932.
- Lee J, Lee I. 2010. Regulation and function of SOC1, a flowering pathway integrator. *Journal of Experimental Botany* 61: 2247–2254.
- Lee J, Oh M, Park H, Lee I. 2008. SOC1 translocated to the nucleus by interaction with AGL24 directly regulates leafy. *The Plant Journal* 55: 832–843.
- Li W, Tian Z, Yu D. 2015. WRKY13 acts in stem development in *Arabidopsis thaliana*. *Plant Science* 236: 205–213.
- Lin G, Zhou Y, Li M, Fang Y. 2018. Histone 3 lysine 36 to methionine mutations stably interact with and sequester SDG8 in *Arabidopsis thaliana*. *Science China Life Sciences* 61: 225–234.
- Lu L, Chen X, Qian S, Zhong X. 2018. The plant-specific histone residue Phe41 is important for genome-wide H3.1 distribution. *Nature Communications* 9: 630.
- de Lucas M, Pu L, Turco G, Gaudinier A, Morao AK, Harashima H, Kim D, Ron M, Sugimoto K, Roudier F *et al.* 2016. Transcriptional regulation of *Arabidopsis* Polycomb repressive complex 2 coordinates cell-type proliferation and differentiation. *Plant Cell* 28: 2616–2631.
- Mandel T, Landau U, Kaplan T, Williams LE. 2022. The H3K27me3 epigenetic mark is crucial for callus cell identity and for the acquisition of new fate during root and shoot regeneration. *bioRxiv*. doi: 10.1101/2022.05.12.491615.
- Mozgova I, Hennig L. 2015. The Polycomb group protein regulatory network. *Annual Review of Plant Biology* 66: 269–296.
- Mozgova I, Köhler C, Hennig L. 2015. Keeping the gate closed: functions of the Polycomb repressive complex PRC2 in development. *The Plant Journal* 83: 121–132.
- Mozgova I, Munoz-Viana R, Hennig L. 2017. PRC2 represses hormone-induced somatic embryogenesis in vegetative tissue of *Arabidopsis thaliana*. *PLoS Genetics* 13: e1006562.
- Murashige T, Skoog F. 1962. A revised medium for rapid growth and bio assays with tobacco tissue cultures. *Physiologia Plantarum* 15: 473–497.
- Ohashi-Ito K, Oda Y, Fukuda H. 2010. *Arabidopsis* VASCULAR-RELATED NAC-DOMAIN6 directly regulates the genes that govern programmed cell death and secondary wall formation during xylem differentiation. *Plant Cell* 22: 3461–3473.
- Pajoro A, Biewers S, Dougali E, Leal Valentim F, Mendes MA, Porri A, Coupland G, Van de Peer Y, van Dijk AD, Colombo L *et al.* 2014. The (r) evolution of gene regulatory networks controlling *Arabidopsis* plant reproduction: a two-decade history. *Journal of Experimental Botany* 65: 4731–4745.
- Pengelly AR, Copur Ö, Jäckle H, Herzig A, Müller J. 2013. A histone mutant reproduces the phenotype caused by loss of histone-modifying factor Polycomb. *Science* 339: 698–699.
- Poulios S, Vlachonasis KE. 2018. Synergistic action of *GCN5* and *CLAVATA1* in the regulation of gynoecium development in *Arabidopsis thaliana*. *New Phytologist* 220: 593–608.

- Pradhan Mitra P, Loqué D. 2014. Histochemical staining of *Arabidopsis thaliana* secondary cell wall elements. *Journal of Visualized Experiments* 51381.
- Probst AV, Desvoves B, Gutierrez C. 2020. Similar yet critically different: the distribution, dynamics and function of histone variants. *Journal of Experimental Botany* 71: 5191–5204.
- Rahimi A, Karami O, Lestari AD, de Werk T, Amakorová P, Shi D, Novák O, Greb T, Offringa R. 2022. Control of cambium initiation and activity in *Arabidopsis* by the transcriptional regulator AHL15. *Current Biology* 32: 1764–1775.
- Ratcliffe OJ, Kumimoto RW, Wong BJ, Riechmann JL. 2003. Analysis of the *Arabidopsis* MADS AFFECTING FLOWERING gene family: MAF2 prevents vernalization by short periods of cold. *Plant Cell* 15: 1159–1169.
- Sanders D, Qian S, Fieweger R, Lu L, Dowell JA, Denu JM, Zhong X. 2017. Histone lysine-to-methionine mutations reduce histone methylation and cause developmental pleiotropy. *Plant Physiology* 173: 2243–2252.
- Schalk C, Cognat V, Graindorge S, Vincent T, Voinnet O, Molinier J. 2017. Small RNA-mediated repair of UV-induced DNA lesions by the DNA DAMAGE-BINDING PROTEIN 2 and ARGONAUTE 1. *Proceedings of the National Academy of Sciences, USA* 114: 201618834.
- Schindelin J, Arganda-Carreras I, Frise E, Kaynig V, Longair M, Pietzsch T, Preibisch S, Rueden C, Saalfeld S, Schmid B *et al.* 2012. Fiji: an open-source platform for biological-image analysis. *Nature Methods* 9: 676–682.
- Schmitges FW, Prusty AB, Faty M, Stutzer A, Lingaraju GM, Aiwezian J, Sack R, Hess D, Li L, Zhou S *et al.* 2011. Histone methylation by PRC2 is inhibited by active chromatin marks. *Molecular Cell* 42: 330–341.
- Schuettengruber B, Chourrout D, Vervoort M, Leblanc B, Cavalli G. 2007. Genome regulation by Polycomb and trithorax proteins. *Cell* 128: 735–745.
- Sequeira-Mendes J, Araguez I, Peiro R, Mendez-Giraldez R, Zhang X, Jacobsen SE, Bastolla U, Gutierrez C. 2014. The functional topography of the *Arabidopsis* genome is organized in a reduced number of linear motifs of chromatin states. *Plant Cell* 26: 2351–2366.
- Servet C, Conde e Silva N, Zhou D-X. 2010. Histone acetyltransferase AtGCN5/HAG1 is a versatile regulator of developmental and inducible gene expression in *Arabidopsis*. *Molecular Plant* 3: 670–677.
- Shi L, Wang J, Hong F, Spector DL, Fang Y. 2011. Four amino acids guide the assembly or disassembly of *Arabidopsis* histone H3.3-containing nucleosomes. *Proceedings of the National Academy of Sciences, USA* 108: 10574–10578.
- Shu J, Chen C, Li C, Cui Y. 2020. The complexity of PRC2 catalysts CLF and SWN in plants. *Biochemical Society Transactions* 48: 2779–2789.
- Shu J, Chen C, Thapa RK, Bian S, Nguyen V, Yu K, Yuan Z-C, Liu J, Kohalmi SE, Li C *et al.* 2019. Genome-wide occupancy of histone H3K27 methyltransferases CURLY LEAF and SWINGER in *Arabidopsis* seedlings. *Plant Direct* 3: e00100.
- Singh RK, Liang D, Gajjalaihvari UR, Kabbaj M-HM, Paik J, Gunjan A. 2010. Excess histone levels mediate cytotoxicity *via* multiple mechanisms. *Cell Cycle* 9: 4236–4244.
- Smyth D, Bowman J, Meyerowitz E. 1990. Early flower development in *Arabidopsis*. *Plant Cell* 2: 755–767.
- Talbot MJ, White RG. 2013. Methanol fixation of plant tissue for scanning electron microscopy improves preservation of tissue morphology and dimensions. *Plant Methods* 9: 36.
- Taylor-Teeple M, Lin L, de Lucas M, Turco G, Toal TW, Gaudinier A, Young NF, Trabucco GM, Veling MT, Lamothe R *et al.* 2015. An *Arabidopsis* gene regulatory network for secondary cell wall synthesis. *Nature* 517: 571–575.
- Trovato M, Patil V, Gehre M, Noh KM. 2020. Histone variant H3.3 mutations in defining the chromatin function in mammals. *Cell* 9: 2716.
- Villette C, Zumsteg J, Schaller H, Heintz D. 2018. Non-targeted metabolic profiling of BW312 *Hordeum vulgare* semi dwarf mutant using UHPLC coupled to QTOF high resolution mass spectrometry. *Scientific Reports* 8: 13178.
- Xu C, Cao H, Zhang Q, Wang H, Xin W, Xu E, Zhang S, Yu R, Yu D, Hu Y. 2018. Control of auxin-induced callus formation by bZIP59–LBD complex in *Arabidopsis* regeneration. *Nature Plants* 4: 108–115.
- Yamaguchi M, Mitsuda N, Ohtani M, Ohme-Takagi M, Kato K, Demura T. 2011. VASCULAR-RELATED NAC-DOMAIN 7 directly regulates the expression of a broad range of genes for xylem vessel formation: direct target genes of VND7. *The Plant Journal* 66: 579–590.
- Yan A, Borg M, Berger F, Chen Z. 2020. The atypical histone variant H3.15 promotes callus formation in *Arabidopsis thaliana*. *Development* 147: dev184895.
- Zhang J, Eswaran G, Alonso-Serra J, Kukucoglu M, Xiang J, Yang W, Elo A, Nieminen K, Damén T, Joung J-G *et al.* 2019. Transcriptional regulatory framework for vascular cambium development in *Arabidopsis* roots. *Nature Plants* 5: 1033–1042.
- Zhang S, Wang D, Zhang H, Skaggs MI, Lloyd A, Ran D, An L, Schumaker KS, Drews GN, Yadegari R. 2018. FERTILIZATION-INDEPENDENT SEED-Polycomb repressive complex 2 plays a dual role in regulating type I MADS-box genes in early endosperm development. *Plant Physiology* 177: 285–299.
- Zhang W, Zhang X, Xue Z, Li Y, Ma Q, Ren X, Zhang J, Yang S, Yang L, Wu M *et al.* 2019. Probing the function of metazoan histones with a systematic library of H3 and H4 mutants. *Developmental Cell* 48: 406–419.
- Zhang X, Ménard R, Li Y, Coruzzi GM, Heitz T, Shen W-H, Berr A. 2020. *Arabidopsis* SDG8 potentiates the sustainable transcriptional induction of the pathogenesis-related genes PR1 and PR2 during plant defense response. *Frontiers in Plant Science* 11: 277.
- Zhou J, Zhong R, Ye Z-H. 2014. *Arabidopsis* NAC domain proteins, VND1 to VND5, are transcriptional regulators of secondary wall biosynthesis in vessels. *PLoS ONE* 9: e105726.

Supporting Information

Additional Supporting Information may be found online in the Supporting Information section at the end of the article.

Fig. S1 Sequences of the H3.3- and H3.3^{K27A}-encoding transgenes (designed from the *HTR5* sequence) and of the H3.3-encoding *HTR5* (At4g40040).

Fig. S2 Selection of sets of H3.3 and H3.3^{K27A} lines with comparable transgene expression and analysis of H3 protein accumulation in the soluble vs insoluble fraction.

Fig. S3 H3.3^{K27A} lines flower early in mid-day and long-day conditions.

Fig. S4 Expression analysis of key flowering genes in the H3.3 control (H3.3 #C) and H3.3^{K27A} (H3.3^{K27A} #B and #37) compared to curly leaf (*clf-2*) mutant and Ler wild-type plants.

Fig. S5 Expression analysis of flowering genes in the H3.3 control (H3.3 #C) and H3.3^{K27A} (H3.3^{K27A} #B and #37) compared to Ler wild-type plants.

Fig. S6 Meristem size and organ initiation analyses of the H3.3 and H3.3^{K27A} lines.

Fig. S7 H3.3^{K27A} lines proliferate calli faster, and fail to regenerate shoots on shoot inducing medium.

Fig. S8 Cell elongation and stomata patterning are affected in the H3.3^{K27A} lines.

Fig. S9 Additional stem morphology analyses of the H3.3^{K27A} lines: epidermis and cortex.

Fig. S10 Additional stem morphology analyses of the H3.3^{K27A} lines: epidermis and cortex layer measurements.

Fig. S11 Analysis of H3 mark abundance in H3.3^{K27A} vs H3.3 expressing lines.

Fig. S12 2-D score plot for principal component analysis showing the differential transcriptomes between WT, H3.3 #C and H3.3^{K27A}#B.

Fig. S13 Gene ontology of genes up-regulated in the H3.3^{K27A} plants and enrichment in transcription factor classes.

Fig. S14 Gene ontology of genes down-regulated in the H3.3^{K27A} plants and proportions of transcription factors in the various populations of down-regulated genes in overlap with H3K27me3 and or *emf2* targets.

Fig. S15 Analysis of expression and the enrichment for H3K27me3 mark at selected genes in the H3.3 control (H3.3 #C) and H3.3^{K27A} (H3.3^{K27A} #B and #37) plants.

Fig. S16 Metabolite profiles of H3.3^{K27A} #B diverge from that of WT and H3.3 #C.

Methods S1 Supporting information for the Material and methods section.

Table S1 List and sequences of oligonucleotides used in the study.

Table S2 RNA-seq data with the full list of *Arabidopsis thaliana* genes and log₂FC between H3.3^{K27A} (#B) and H3.3 (#C) calli.

Table S3 Overlap between the lists of H3.3^{K27A} up-regulated genes and H3K27me3 targets or/and *emf2* up-regulated genes.

Table S4 Overlap between the lists of H3.3^{K27A} down-regulated genes and H3K27me3 targets or/and *emf2* down-regulated genes.

Table S5 Subsets of genes mis-regulated in H3.3^{K27A}, mapped to KEGG for the phenylpropanoid biosynthesis, hormone signaling pathways and those acting in cell wall and vasculature development.

Table S6 Metabolomics data with the full list of *Arabidopsis thaliana* genes and log₂FC between H3.3^{K27A} (#B) and H3.3 (#C) lines.

Table S7 Metabolomics data for H3.3^{K27A} vs H3.3, mapped to KEGG for the phenylpropanoid biosynthesis pathways.

Please note: Wiley is not responsible for the content or functionality of any Supporting Information supplied by the authors. Any queries (other than missing material) should be directed to the *New Phytologist* Central Office.